HELMUT SCHMIDT
UNIVERSITÄT

Universität der Bundeswehr Hamburg

Johannes Hallier

Design of an ultrafast laser pulse shaper using a spatial light modulator and evolutionary strategies

2

Fachbereich Elektrotechnik
Laser Engineering and Materials Science

Univ.-Prof. Dr. rer. nat. Hermann Harde

Helmut Schmidt University
University of the Federal Armed Forces Hamburg
Postfach 70 08 22
22008 Hamburg

Telefon: (040) 6541 - 2147
Telefax: (040) 6541 - 3764

Email: harde@hsu-hh.de
Internet: http://www.hsu-hh.de/laser/

Erklärung

Hiermit erkläre ich,

Johannes Hallier, Matr.Nr.:793090,

dass ich die vorliegende Diplomarbeit selbständig ohne fremde Hilfe angefertigt habe und keine anderen Quellen als die angegebenen verwendet habe.

Hanover, den 28.02.2007 .....

Contents

List of Symbols

∇	Nabla operator $\nabla = \frac{\partial}{\partial x} + \frac{\partial}{\partial y} + \frac{\partial}{\partial z}$
c	Speed of light
U	Wave amplitude
$\vec{r}$	Position vector
t	Time
j	Imaginary unit
ω	Angular frequency $\omega = 2\pi f$
k	Wave number
∇_T	Transverse nabla operator $\nabla_T = \frac{\partial}{\partial x} + \frac{\partial}{\partial y}$
A	Amplitude of electromagnetic wave
ρ	Radius in cartesian coordinates $\rho^2 = x^2 + y^2$
z_0	Rayleigh range
W	Beam diameter
R	Beam radius
ξ	Phase retardance of wavefronts
λ	Wavelength
d	Grating groove spacing
G	Grating groove frequency
α	Input angle at grating
β	Output angle at grating
m	Diffraction order
N	Total number of illuminated grooves
R	Grating resolving power
$\Delta\lambda$	Resolvable wavelength difference
γ_{blaze}	Blaze angle of ruled gratings
n	Index of refraction
φ	Angle of light to refractive material
f	Focal length
R_{SM}	Spherical mirror radius
$E(\omega)$	Electric field in frequency domain
$e(t)$	Electric field in time domain
$H(\omega)$	Transfer function
Φ	Phase of electromagnetic wave

w	Width of spectral components on SLM
P	Power
T	Transmission
$m(x)$	Spatial mask pattern
$B_{n,g}, c_n$	Filter coefficients for SLM
δ	Dirac function
$rect$	Rectangular function
Ω	Difference of frequency components to center frequency
$\overline{z}$	Distance of mask to focal plane
a	Spot size of beam

Chapter 1

Introduction

Ultrafast laser pulses in the femtosecond time domain have changed many existing and opened new fields since their invention in the 1980's. Improvements in the techniques of the used lasers and compression systems have resulted in the creation of pulses consisting of only a few femtoseconds, or a few cycles of visible light[1]. Along with shorther pulses have come techniques to modulate its amplitude and phase. Possible applications have appeared in the field of optical communication or in the control of chemical reactions, also called "femtocontrol". For communication purposes, an arbitrarily shaped femtosecond pulse can be used to carry data modulated with WDM[2] or CDMA[3] techniques, which have in common that the desired shape of the pulse is known before sending it through the pulse shaper. [ShG02]
For "femtocontrol" experiments, this is usually not the case. Here, a feedback parameter from the experiment can serve as an indicator for the suitability of the used pulse. By using genetic algorithms, the shaping parameters can be optimized to find the best solution. This is necessary, because the systems are too complex to be described by a model that could help to find the best solutions. Then, studying the optimum solution leads to a deeper understanding of innerlying effects in molecular reactions [Lup04].

In this work, a pulse shaper was developed that needed to be as flexible as possible, as potential requirements for different experiments may vary from time to time. Therefore, a control program was written which allows to shape a pulse in time domain, in frequency domain, and also to integrate a feedback parameter for a genetic algorithm, which is a very flexible solution, since only the measurement of the feedback parameter needs to be changed and integrated into the control program. For the calibration purpose, it was required to have an easy-to-use procedure that, even if the setup is moved and needs to be recalibrated, will allow to obtain the same results as measured at a

[1] light at $\lambda = 750nm$ has a cycle of $t = 2.5fs$
[2] Wavelength Division Multiplexing
[3] Code Division Multiple Access

different place. Since for most flexibility, the pulse shaper needs to be moved to the experiment, and not the other way around, this can become very important.

The outline of the thesis is as follows: First, the theoretical background required for pulse shaping is given. In greater detail, the general design parameters required for the setup are illustrated and then applied to the setups used for this work. Then, control program and its subprograms are explained. Finally, some example measurements demonstrate the capability of the pulse shaper to generate defined pulse shapes and some suggestions are given to improve and extend the work.

Chapter 2

Fundamental principles

A pulse shaper uses basic optical components to disperse and focus the different wavelength components to the Fourier plane, where the amplitude and phase of different spectral components can be individually modified. In this paragraph, the components of the setup and the principles for modifying the pulse shape in time and frequency domain will be introduced.

2.1 Optics

2.1.1 Beam optics

A laser beam is an electromagnetic wave which obeys the wave equation

$$\nabla^2 U - \frac{1}{c^2}\frac{\partial^2 U}{\partial t^2} = 0. \tag{2.1}$$

Assuming a harmonically oscillating wave in time which spatial amplitude can, in general, be described using a complex phasor

$$U(\vec{r}, t) = U(\vec{r})\, e^{j\omega t}, \tag{2.2}$$

which includes the amplitude and the phase of the wave at time $t = 0$. Inserting this into the wave equation leads to

$$(\nabla^2 + \frac{\omega^2}{c^2})\, U(\vec{r})\, e^{j\omega t} = 0, \tag{2.3}$$

where $e^{j\omega t} \neq 0 \; \forall \; t$. Substituting $k = \frac{\omega}{c}$ yields

$$(\nabla^2 + k^2)\, U(\vec{r}) = 0. \tag{2.4}$$

This is the Helmholtz equation which contains solutions such as the planar or the spherical wave. A laser beam, however, is not a completely planar wave. Every beam

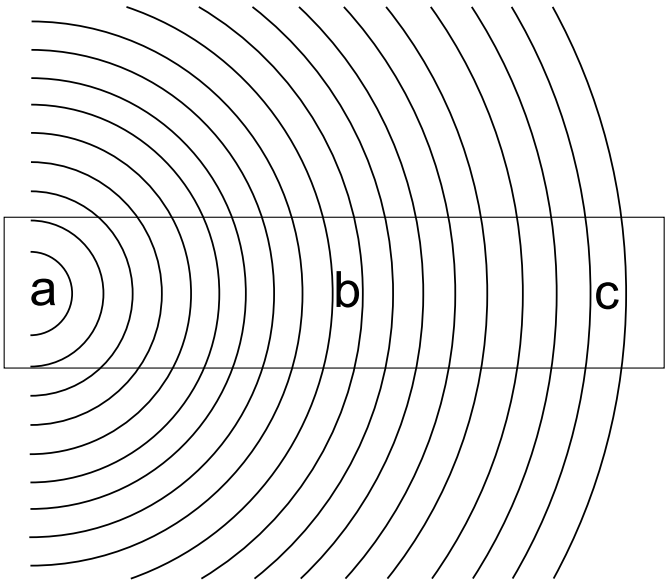

Figure 2.1: Wave at different distances within a small cylinder around the axis **(a)** Spherical wave **(b)** ellipsoidal wave **(c)** paraxial wave. Compare at [SaT91].

experiences a certain angle of divergence, although the angle may be very small such that the divergence is only visible at great distances from the laser source. The wavefronts differ from the planar wave

$$U(\vec{r}) = A\, e^{-jkz} \tag{2.5}$$

and become slightly curved, which can be approximated using a spherical wave from a distant source within a small diameter around the propagation axis (see figure 2.1).

Taking the planar wave equation, a paraxial wave can be described using the slowly varying amplitude approximation (SVA)

$$U(\vec{r}) = A(\vec{r})e^{-jkz}, \tag{2.6}$$

which means that $\Delta A \ll A$ within a wavelength λ. Applying 2.6 together with the SVA on the wave equation result in the paraxial Helmholtz equation for the complex amplitude $A(\vec{r})$,

$$\nabla_T^2 A - j2k\frac{\partial A}{\partial z} = 0,\ \nabla_T^2 = \frac{\partial^2}{\partial x^2} + \frac{\partial^2}{\partial y^2} \tag{2.7}$$

which has several analytical solutions. One of them is the Gaussian beam with the complex amplitude

$$A(\vec{r}) = \frac{A_0}{z + jz_0}\, e^{-jk\frac{\rho^2}{2q(z)}} \tag{2.8}$$

where z_0 is the Rayleigh range for which the diameter of the pulse does not exceed $\sqrt{2}$ times the minimum beam radius W_0. Overall, 2.6 can be written as

$$U(r) = \frac{A_0}{jz_0}\,\frac{W_0}{W(z)}\,e^{-\frac{\rho^2}{W^2(z)}}\,e^{-jkz-jk\frac{\rho^2}{2R(z)}+j\xi(z)}. \tag{2.9}$$

with

$$W_0 = \sqrt{\frac{\lambda z_0}{\pi}} \tag{2.10}$$

$$W(z) = W_0\sqrt{1+(\frac{z}{z_0})^2} \tag{2.11}$$

$$R(z) = z(1+(\frac{z}{z_0})^2) \tag{2.12}$$

$$\xi(z) = \arctan(\frac{z}{z_0}), \tag{2.13}$$

where $W(z)$ is the beam radius within which the intensity decreases to $\frac{1}{e^2}$ of its peak value, R(z) describes the curvature of the beam's wavefronts under the paraxial approximation and $\xi(z)$ is the phase retardation compared to a planar wave, as different points of the wavefront reach the position of a comparable planar wavefront at different times [SaT91].

2.1.2 Diffraction grating

Gratings are based on the principle that a beam of a finite width, which is reflected from a mirror-like surface, will only experience constructive interference if the different spatial components of the beam diameter have discrete differences that match multiples of the wavelength of the incident beam. If the input beam is a pulse containing a spectrum of different wavelengths, each wavelength will be dispersed at a different angle, leading to a spatial dispersion of the spectral components. Therefore, the surface of a grating is made of small grooves, each of them having the same angle to the grating plane. Figure 2.2 shows the principle of a grating with an incident beam and a reflected beam at angle α and β, respectively.

The reflected beam of angle β shows constructive interference if two components from different grooves of the grating have a difference in wavelength of

$$\Delta\lambda = \Delta\lambda_2 - \Delta\lambda_1 = m\lambda. \tag{2.14}$$

Using the relations

$$\sin(\alpha) = \frac{\Delta\lambda_1}{d} \tag{2.15}$$

$$\sin(\beta) = \frac{\Delta\lambda_2}{d} \tag{2.16}$$

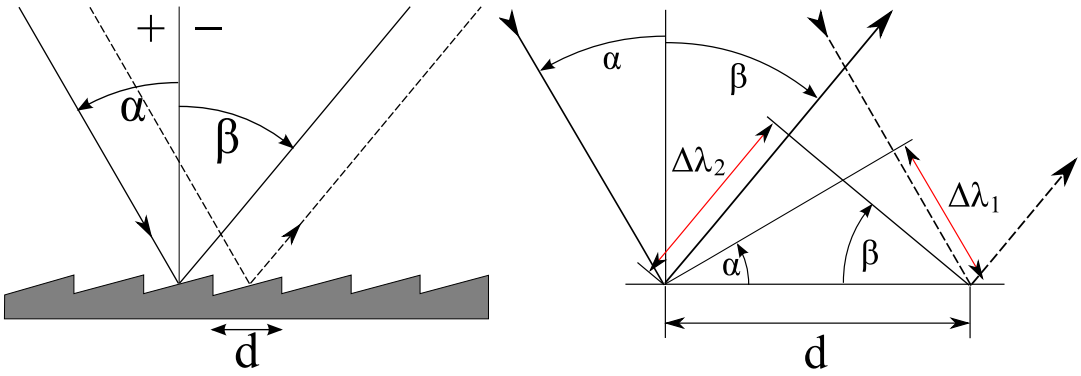

(a) Definitions on a grating (b) Wavefront interference

Figure 2.2: Principle of a diffraction grating

and the groove frequency $G = \frac{1}{d}$ yields the grating equation

$$\sin(\beta) - \sin(\alpha) = mG\lambda. \tag{2.17}$$

Typical gratings are produced by either cutting the surface pattern (ruled gratings) or using holographic procedures, where the pattern becomes sinusoidal (resulting interference pattern from two laser beams). A coating for specific wavelengths can be applied in order to increase the efficiency due to higher reflectivity, as gold is more suitable than Aluminum for infrared applications, for example. Usually, one wants to use the grating in one specific diffraction order m only, e.g. $m = -1$, and the efficiency should be as high as possible for this specific order.
By differentiating the grating equation, the angular dispersion

$$D = \frac{mG}{\cos(\beta)}, \tag{2.18}$$

can be obtained, which is proportional to the groove frequency. Another important parameter is the resolving power

$$R = \frac{\Delta\lambda}{\lambda} = mN, \tag{2.19}$$

which defines the ability to separate adjacent spectral lines. $\Delta\lambda$ is the required resolvable wavelength difference and N defines the total number of grooves illuminated on the grating. Therefore, a higher groove frequency, but also a larger beam diameter on the grating improve the resolution.
Ruled gratings and some holographic gratings are blazed, which defines the angle of the grooves to the grating surface. For holographic gratings, an ion-etching procedure is applied which changes their sinusoidal to a sawtooth groove profile. Used at a Littrow

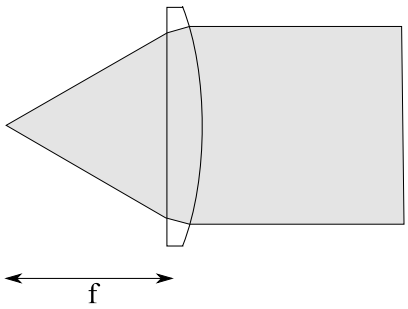

Figure 2.3: Plano-convex lens

configuration ($\alpha \approx \beta \approx \gamma_{blaze}$) often maximizes their efficiency. Even more important for the grating efficiency is the polarization of the incoming light. Performance curves, usually showing the relative power in the desired diffraction order, are therefore often measured for a polarization perpendicular (S-Plane) or parallel (P-Plane) to the groove surface, which significantly changes the efficiency, especially the wavelength range which they are designed for [PaL05].

2.1.3 Lens

A lens is made of a dispersive material with a different refractive index than air. Depending on the shape, lenses can either diverge or focus light. Therefore, their surface is either formed convex, planar or concave. Often, glass is used with n $\approx$ 1.5. Light enters the medium at an angle φ_1 and is refracted to an angle φ_2 according to Snell's Law

$$n_1 \sin \varphi_1 = n_2 \sin \varphi_2. \tag{2.20}$$

Concave lenses spread light, whereas convex lenses collect and focus light. The latter can be made of two convex surfaces, but combinations of planar and convex surfaces are also available, which reduce the angle of the surface to light entering the lens and therefore minimizing optical errors. Parallel light entering a convex lens will be focused at the focal point, and ideally having a zero diameter (figure 2.3). However, using a laser beam under the paraxial approximations of section 2.1.1, the beam diameter at the focal point will not be zero, but finite. Assuming a well collimated beam with $z_0 \gg f$, the beam focuses at the focal length f with a radius

$$W_0' = \frac{\lambda}{\pi W_0} f \tag{2.21}$$

Simple, singlet lenses are usually designed for monochromatic light. However, the refractive index of a medium is usually wavelength dependent. Different wavelength

components will be refracted to different angles in the medium, leading to beam divergence and spatial errors. This phenomenon is called chromatic aberration and can be reduced by using a lens of different materials. A so-called achromatic doublet has two materials, whereas the second one compensates for errors of the first and keeps the wavelength components closely together around the focal point of the lens. Therefore, optical errors will be reduced.

2.1.4 Spherical mirror

Comparable to convex lenses, spherical mirrors collect light from one source and focus it on a specific point depending on the radius of the mirror,

$$f = -\frac{R_{SM}}{2}. \tag{2.22}$$

which is valid under the paraxial approximation [KlF86]. In contrast to lenses, the incoming light does not travel through the medium (in case of metallic front surface mirrors) and therefore chromatic errors due to a different diffraction of spectral components do not occur. These errors have a large influence on pulses of less than 100 fs FWHM (full width half maximum). Achromatic lenses do not significantly reduce the errors, as they introduce CPD (cubic phase dispersion), which also broadens the pulse [RWL92]. Therefore, the use of mirrors instead of lenses is preferred for a flexible setup suitable for short pulses. Spherical mirrors, however, are not free from errors.

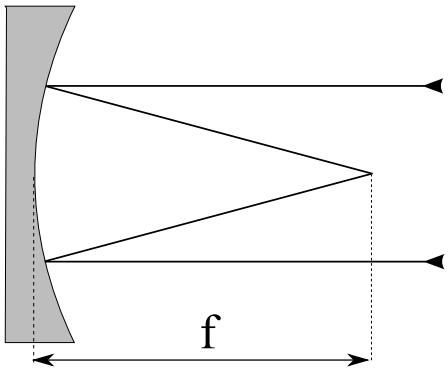

Figure 2.4: Spherical mirror

The perfect shape of a concave mirror is paraboloidal, whereas parallel light will be perfectly focused to a single point. A spherical mirror is easier to produce, but does not focus parallel light perfectly. However, using the paraxial approximation (2.6), a spherical mirror is a paraboloid reflector to first order. The angles between incoming and outgoing light should be small to avoid off-axis aberrations.

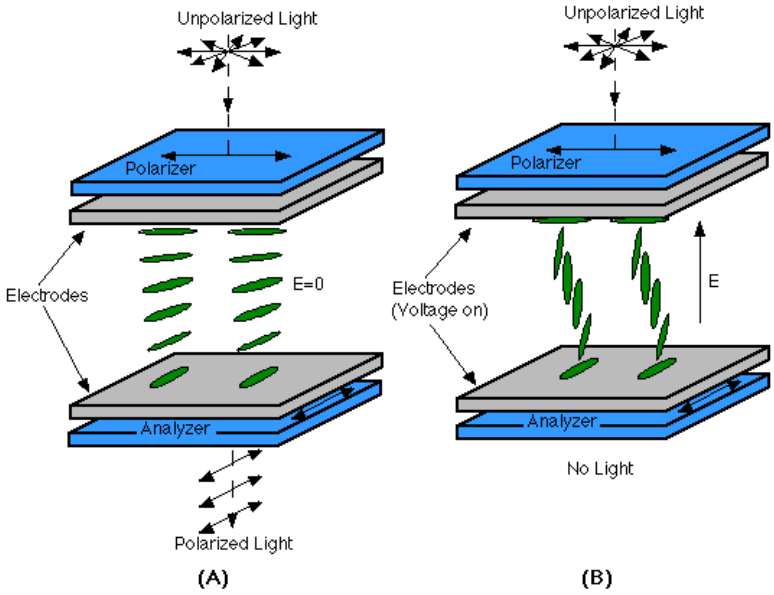

Figure 2.5: Twisted nematic crystals **(a)** without voltage applied, light changes polarization according to the crystals direction **(b)** a voltage causes the molecules to align along the electric field and no light transmits [ChC07]

.

2.2 Spatial Light Modulator

Also called a Liquid Crystal Modulator (LCM), a Spatial Light Modulator (SLM) is equipped with an array of liquid crystals, which is a liquid in a state that has crystal properties, like uniformity and alignment of molecules, as well. Unlike crystals, the alignment of molecules can easily be changed by applying low voltages. Here, the crystal array is aligned along the x axis, the vertical axis of each pixel is the y axis, and the z axis is the direction of light travelling through the device. The crystals are molecules shaped ellipsoidal, with one axis larger than the other.[Cam04].

There are two ways of using a LCM, as a Phase or as an Amplitude modulator. The crystal structure is slightly different for both. Phase modulation is achieved by applying a voltage across the length of the SLM. The crystals tilt from their idle state and cause a change of the refractive index for y-polarized light (see figure 2.6). Thus, the phase of the beam will be changed, as the beam is delayed when passing through the crystal. This effect is wavelength dependent, but as each pixel only has a very small part of the whole spectrum, the wavelength can be assumed constant over the width of a pixel. The phase change as a function of voltage is nonlinear and is usually given

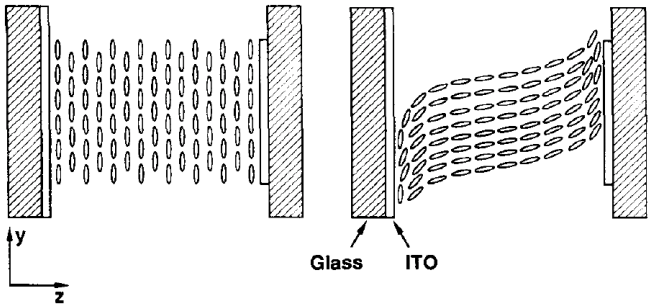

Figure 2.6: Liquid crystals for phase modulation. In idle state, the crystals are aligned along axis y. After applying a voltage across the length z, the crystals tilt and cause a change in the refractive index for y-polarized light [WLP92]

in the documentation of a SLM or can be measured.

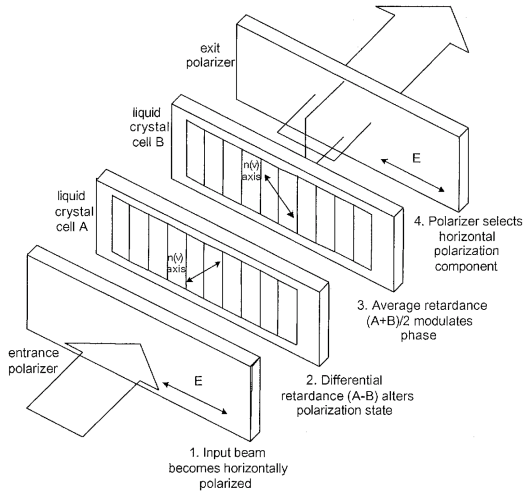

Figure 2.7: Phase and Amplitude Modulation in a SLM in transmission mode [Cam04]

An amplitude modulator uses nematic crystals, which have the property to be naturally aligned in one direction, with little variation over different molecules. This direction is called the director. The incoming light is horizontally polarized with an entrance polarizer. When passing through the crystals, the beam changes its polarization as the crystals change the orientation of their director (figure 2.5 a). If the structure was created such that the directors rotate by 90° over the length of the modulator, the light would experience a shift from horizontal to vertical polarization. After the crystals, an exit polarizer ensures that only the remaining horizontally polarized components

leave the crystal, and eliminates the vertically polarized part of the beam. If the light is completely shifted to vertical polarization, the transmission will drop to zero. In between, any value can be adjusted [Tys00]. Figure 2.7 shows a SLM with a phase and an amplitude mask (dual mode). The device can also be used in reflection mode, if a mirror is attached after the second mask. However, going through the mask two times, any effect on the beam will be doubled, which allows higher phase modulation rates.

2.3 Genetic algorithms

Optimization problems in complex systems are sometimes hard to handle, if almost no information is present about how a change of a parameter influences the solution. Comparable to the natural selection process in nature, where the genetic parameters change over generations to adopt best to the natural conditions. Therefore, the parameters that influence the solution are sometimes called "chromosomes". An initial set of "chromosomes" is created and serves as start solutions, which are used to calculate the optimizing function, which is also called "fitness function" or evaluation functon, as it describes how well the "chromosomes" adopt to their enviroment. The fitness factor, which is higher for better solutions, is used for the next step, the selection. Here, the "fittest" of the solutions are being selected, which can be compared to the misleading term of "survival of the fittest". Therefore, the sum of all fitness factors is calculated, and a probability for each chromosome calculated, which relates its fitness to the overall fitness. Then, a cumulative probability for each chromosome is calculated, whereas the last chromosome sums all probabilites and equals 1. A random value between 0 and 1 selects a chromosome for the new generation, whereas higher probabilites increase the "share" of the space between 0 and 1, and therefore have a higher probability to be selected. When this process is iterated pop_size times, a new generation has been selected. Apparently, some "fitter" solutions can be selected more than once. After that, the solutions are being mixed in the crossover process. Here, individual, equal parts of the "chromosomes" are exchanged. An example of a crossover process is shown in figure 2.8. A randomly selected part of the "parent" solutions is exchanged and results in new, offspring solutions. Then, the third step, the mutation process, selects random bits of the binary solution and swaps them. A "0" turns to a "1" and a "1" to a "0". This process is important for the solutions to escape local minima. An evaluation function with many local minima requires a high probability for a mutation process.
Genetic algorithms require the chromosomes to be binary coded. Often, a problem has to be modified so that the solutions are mapped to binary values to be suitable for a genetic algorithm. The choice of a suitable coding method is very important. In

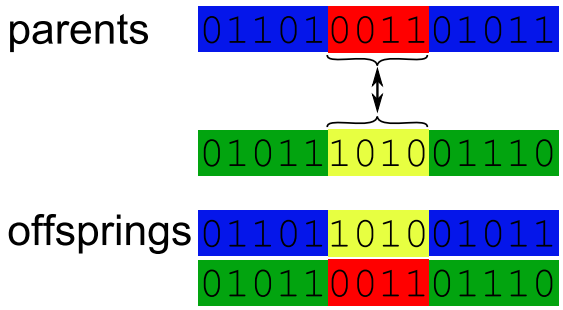

Figure 2.8: The crossover process in Genetic Algorithms. Here, two parts of the parents solutions (red and yellow) are broken out and exchanged to generate offspring solutions. The remaining solution is unchanged.

difference to that, evolutionary programs do not change the coding, but instead apply suitable operators to the parameters [Mic96].

Chapter 3

Pulse Shaping

Femtosecond pulse shaping usually describes the complete, arbitrary manipulation of amplitude and phase of an ultrashort laser pulse, limited by the available bandwidth, power and resolution of the used components. Today, there exist direct and indirect techniques. The first ones modulate a pulse in space and shape the pulse in the time domain, whereas the latter use the Fourier transform to modulate pulses in the frequency domain. Direct space-to-time techniques, for example, use a mask and slit-apparatus to generate pulse trains that can be used in optical communications or other applications [LeW01]. Indirect techniques work in the Fourier domain, where the single frequency components of an ultrafast pulse are spatially separated from each other. A modulation of the amplitude and phase in the frequency domain results in a pulse in time domain determined by its inverse Fourier transform. This chapter describes the fundamentals of the Fourier transform pulse shapers and their different implementations.

3.1 Principle of Fourier transform pulse shaping

The most common implementation of a Fourier transform pulse shaper, also called the 4f-setup, consists of 4 optical components, each of them separated by the focal length of a focussing component such as lenses or spherical mirrors.
The input pulse is spatially dispersed by a reflection grating, which is placed one focal length from a lens or a spherical mirror. The single frequency components will then propagate parallel to each other, as long as the input beam is perfectly collimated, does not diverge significantly and the distances precisely equal the focal length f. Another distance f away, the frequency components will show their minimum beam waist according to the lens equation (2.21). Here, the wave components can be attenuated and retarded, in order to change their amplitude and phase. Therefore, an SLM device, an Acousto-Optic Modulator (AOM) [Wei00] or a fixed mask pattern is used, which is

also suitable for micro-fabricated devices [Thu86]. One focal length further, the second lens or spherical mirror focuses the beam onto the second grating, which, if all angles are symmetric, assembles the outgoing beam [Wei00].
Mathematically, such a pulse shaper can be described using the Fourier transform of the input pulse in time domain $e_{in}(t)$,

$$E_{in}(\omega) = \int_{-\infty}^{\infty} e_{in}(t)\ e^{-j\omega t} dt, \tag{3.1}$$

which can be found at the Fourier plane before the SLM. The SLM modulates amplitude and phase of the signal, and can be represented by the linear transfer function

$$H(\omega) = A(\omega)\ e^{j\phi(\omega)} \tag{3.2}$$

with the amplitude modulation $A(\omega) = \frac{A_{out}(\omega)}{A_{in}(\omega)}$ and the phase factor $\phi(\omega) = \phi_{out}(\omega) - \phi_{in}(\omega)$. The shape of the output waveform in frequency is given by

$$E_{out}(\omega) = H(\omega)\ E_{in}(\omega), \tag{3.3}$$

which can be rewritten in time domain using the inverse Fourier transform, but a different approach is to define the output waveform in time domain, calculate the corresponding $E_{out}(\omega)$, and then calculate the transfer function using the measured input waveform. The transfer function in frequency domain can be mapped to a function in space by a calibration procedure, where the wavelength components impinging on the SLM are mapped to their respective pixels.
Also, the connection of space to frequency has been studied theoretically by Wefers and Nelson [WeN95]. For an SLM with two masks having a perpendicular crystal axis alignment to each other, a filter for one pixel n can be written as

$$B_n = e^{i\frac{1}{2}(\Delta\Phi_1 + \Delta\Phi_2)}\ \cos(\frac{1}{2}(\Delta\Phi_1 - \Delta\Phi_2)). \tag{3.4}$$

This represents a filter for amplitude and phase, and if we consider that, when speaking of transmission, usually the intensity and not the amplitude is meant, a transmission function

$$T = \cos^2(\frac{1}{2}(\Delta\Phi_1 - \Delta\Phi_2)) \tag{3.5}$$

and a phase function

$$\varphi = \frac{1}{2}(\Delta\Phi_1 + \Delta\Phi_2)) \tag{3.6}$$

can be calculated, which allow a definition of an arbitrarily shaped pulse in amplitude and phase.
Using the Fourier transform, the waveform after the SLM can be written as

$$E_{out}(x, \omega) = g(x) E_{in}(\Omega) m(\alpha\Omega) \tag{3.7}$$

with the spatial profile $g(x)$ of the input pulse, the mask pattern m(x), $\Omega = \omega - \omega_{x0}$ and α the first order coefficient, which relates a frequency component to its spatial position on the SLM. The spatial mask filter $m(x)$ can be written as a series of rectangular filters for pixels and gaps,

$$m(x) = \delta(x - x_0) * \sum_{n=-N/2}^{N/2-1} \{((B_n \delta(x - nw)) * rect(\frac{x}{rw}) + (B_g \delta(x - (n + \frac{1}{2}w))) * rect(\frac{x}{1-r}w)\}, \tag{3.8}$$

with the filters $B_{n/g}$ for pixel n and gap g, respectively. The fourier transform of the mask filter can be used to calculate the electric field after the SLM. With two masks separated at an equal distance from the focal plane, the electric field becomes

$$e_{out}(t) = \sum_{n=-\infty}^{\infty} (\frac{c_n^{(1)} + c_n^{(2)}}{2})\, e_{in}(t + n\tau)\, e^{-\frac{n^2\chi^2}{2a^2}(1+(\frac{\pi\lambda a^2 \overline{z}}{2\chi^2 w^2 N^2})^2)}, \tag{3.9}$$

with the coefficients c_n for pixel n, here for both masks, and an exponential term which incorporates spatial effects of the spot size a, the distance of the masks from the focal plane $\overline{z}$, and a factor $\chi = \frac{\cos(\Phi_i)\lambda f}{\cos(\Phi_d) N w}$ with parameters from the optical system [WeN95].

3.2 Design types

The first design introduced used lenses and gratings along one optical line (see figure 3.1). It allows an easy alignment procedure, as there is only one height for the beam throughout the setup, and distances can easily be measured. However, the setup is comparatively large and the lenses may cause problems for ultrashort pulses; the shorter the pulse duration, the less suitable lenses are as they introduce chromatic errors and cubic phase dispersion and therefore broaden the pulse. As a better solution, setups with reflective optics, especially concave/cylindrical mirrors, were introduced.

First, there is the possibility to reflect light directly from the grating onto the mirror, but the distance between both components needs to equal one focal length, which requires the grating to be positioned next to the SLM, as there is no more space for the mount (see figure 3.3). Therefore, a large tilting angle of the mirror is necessary, but this comes with off-axis aberrations. This design type has been tested with a high-resolution SLM [SHF01]. To reduce these errors, and therefore to keep the angles small, a folding mirror is required, which is possible because the spectrum only expands in one dimension. Spectrum and beam can be separated at close distance and the tilt of the mirror does not have to exceed more than 1 to 2 degrees to the optical axis

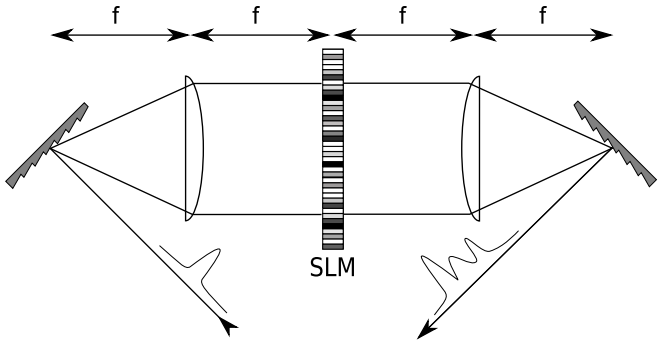

Figure 3.1: 4f-setup with lenses as focusing elements

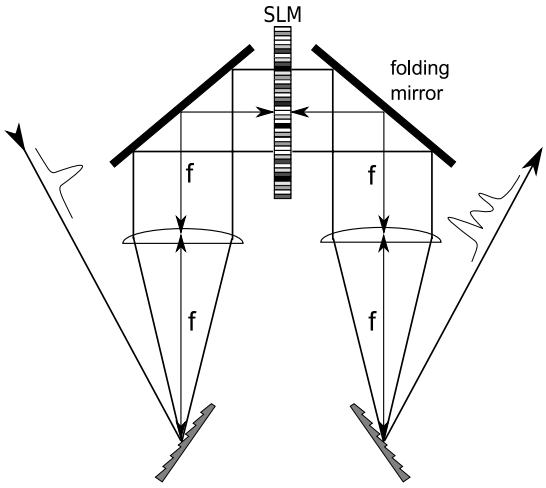

Figure 3.2: Lens setup with folding mirrors

with the two mirrors and the SLM. This setup only requires two focal lengths in one direction, which halves the dimensions of the lens setup (figure 3.4). However, a tilt of the gratings and of the folding mirrors are necessary, as the beams are situated in two planes, the one for the incoming beam which enters above the first mirror, which is also the height of the beam between the two focusing mirrors, and a lower level at the folding mirror. Therefore, the spectrum is deflected downward from the grating to the folding mirror, and then reflected upwards to the focusing mirror. Folding mirrors can also be used with lens setups in order to build a more compact design. However, they need to be larger as the full width of the diffracted pulse will be folded (see figure 3.2). Such a design has been used in an earlier work for a pulse shaper in an amplifying system [Fet99].

Another variation was presented in [PWA03]. Here, one focal length determines the

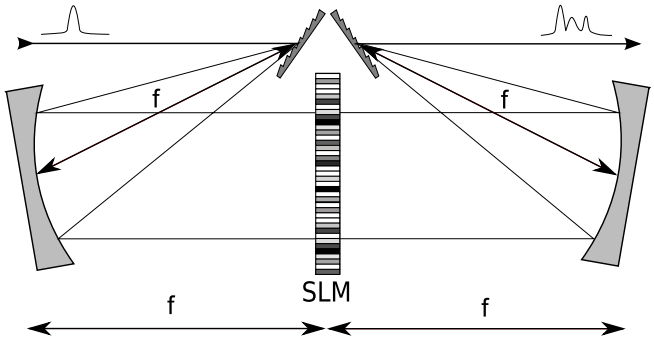

Figure 3.3: Reflective setup with spherical mirrors as focusing elements

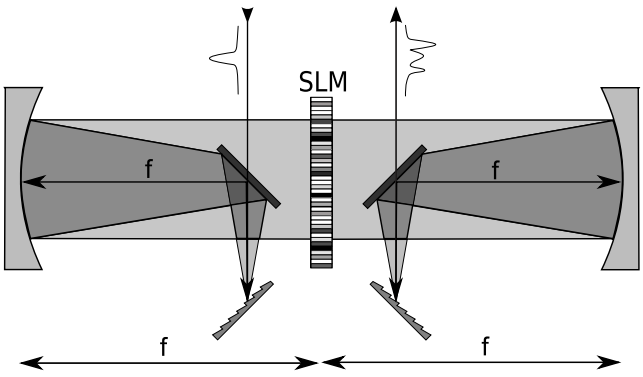

Figure 3.4: Reflective setup with folding mirrors to increase grating efficiency and reduce optical errors

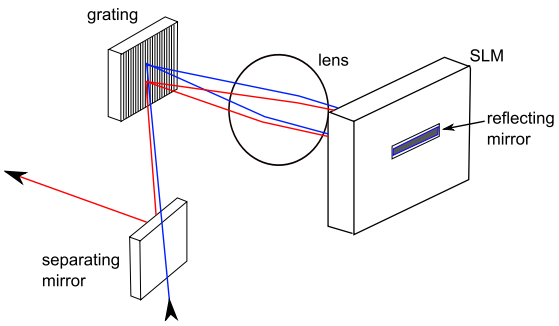

Figure 3.5: A tilt of a mirror immediately after the SLM can separate the incoming beam (blue) from the outgoing beam (red).

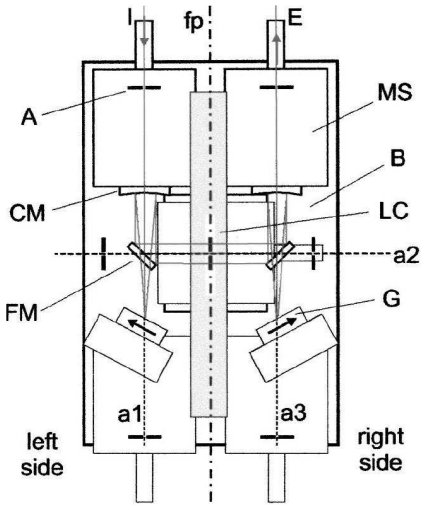

Figure 3.6: Compact reflective setup with high mechanical precision [PWA03]

length of the setup, which is the distance from the grating to the folding mirror. The folding mirrors reflect the whole width of the spectrum and need to be larger. The advantage is that the large width of the whole SLM is completely used for the distance between gratings and focusing mirrors. This setup therefore is extremely compact (figure 3.6). Another possibility to reduce the need of two focal lengths with a reflective folding design is the use of a mirror immediately after the SLM. The spectrum is reflected and passes twice through the SLM which also doubles the amplitude and phase modulation. A slight tilt of the reflecting mirror needs to be introduced to be able to spatially separate the incoming and outgoing beam after the grating, which is now used for dispersion and assembly of the beam (also see figure 3.5).

3.3 Measurement of ultrashort pulses

Laser pulses have originally been measured with photo diodes, but their integration time limits their applicability to lengths in the picosecond domain (ps). Shorter pulses require autocorrelation techniques such as the Frequency Resolved Optical Gating (FROG). The pulse is divided into a reference pulse and a delayed version of itself, which are both focused on a nonlinear crystal. Here, nonlinear effects cause a 'multiplication' of both pulses, resulting in a pulse with doubled frequency. This frequency - measured with a spectrometer - is a result of a second harmonic effect, giving the device its name Second Harmonic Generation (SHG) FROG. A typical setup of a FROG device is shown in figure 3.7, whereas the photomultiplier has to be replaced with a spectrometer. The three measured parameters - time delay, frequency and amplitude

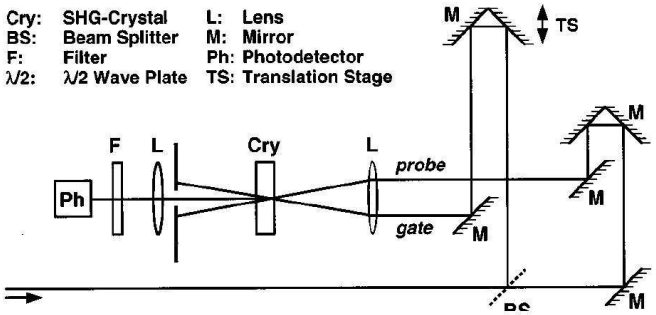

Figure 3.7: Setup of SHG FROG [Tre97]

- are combined in a spectrogram. From this trace, a computer algorithm deducts amplitude and phase in time and frequency domain by iteratively comparing a theoretical with the measured plot and minimizing the error [Tre97]. The FROG has proven to be a reliable device for measuring ultrashort pulses, however, some problems are the necessity of a relatively high power for the SHG-FROG and the comparatively long time to completely characterise a pulse. Other techniques are also available and should be taken into consideration for each individual application.

3.4 Feedback design

If the required pulse characteristics are unknown, or if the calibration does not yield a sufficient accuracy, a feedback design based on evolutionary strategies can be used [BBS97]. A feedback parameter, such as a second harmonic generation signal by a nonlinear crystal, serves as the evalutation function (see section 2.3). If the parameters

for the pattern to shape a desired pulse are unknown, or do not lead to optimum results because of errors or miscalculations, a genetic algorithm can help to find a better solution. Figure 3.8 shows the cycle that includes the algorithm, the upload of a new pixel pattern to the SLM and a measurement (in this case a SHG signal) as a feedback parameter.

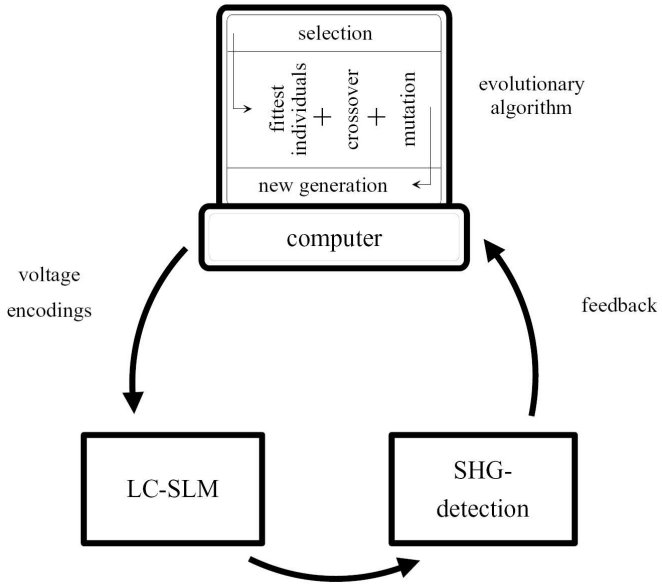

Figure 3.8: Pulse shaping principle with an evolutionary algorithm and a feedback parameter for optimization of the pulse shape [BBS97]

Chapter 4

Design and setup

First, a pulse shaper in a 4f-setup with lenses was experimentally investigated. Later, it was exchanged to a reflective setup with spherical mirrors.

4.1 Design parameters and criteria

A pulse shaper needs to be adapted to the laser source, i.e. center wavelength, spectral width, output polarization and maybe output power. The design was made for a SpectraPhysics Mai Tai® [1] ultrafast laser, which has an output power of about $700mW$ and a pulse width of about $100fs$ around a tunable center wavelength, which was set to $800nm$.
The main criterion for a pulse shaper is the width of the liquid crystal array in the SLM device. On the one hand, a large bandwidth of the pulse should be used, as no frequency components should be lost for an efficient modulation. On the other hand, the resolution increases with a smaller bandwidth, so that each pixel modulates a smaller part of the most important parts of the spectrum concerning the energy. A cut-off criterion is the simplest solution to choose, as only those parts of the spectrum with intensities of more than 2% or 3% of the maximum value contribute enough to be considered important for the shaping of the pulse.
Figure 4.1 shows a spectrum of a pulse from the MaiTai laser, recorded directly after the laser output. In this example, a reasonable wavelength range choice could be from 780-820 nm, in order not to lose any important components and to guarantee a high resolution as well.
After choosing a wavelength range, the grating equation is solved to calculate the diffracted angles for the cut-off wavelengths. To do so, the groove frequency of the grating has to be chosen. In general, a higher groove frequency has a higher diffraction efficiency, which leads to a shorter distance for spreading the spectrum to the required

[1] http://www.newport.com/Mai-Tai-One-Box-TiSapphire-Lasers/368124/1033/catalog.aspx

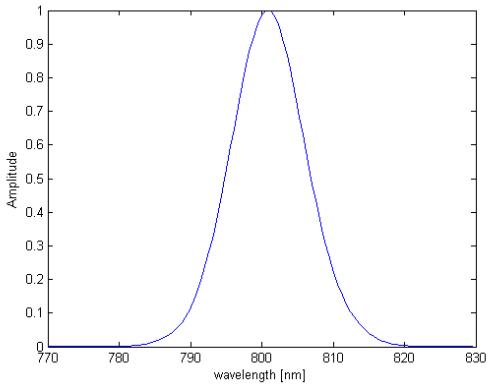

Figure 4.1: Measured spectrum of an unshaped pulse of the MaiTai laser

width. In general, the choice of the grating is not an easy task, as there are only a few gratings with high groove frequencies suitable for wavelengths around the center frequency of our laser. Also, the efficieny curves of the gratings have to be considered, as their dispersion efficiency varies with different types, and they should be most efficient at the design wavelength and match the input polarizers of the SLM device. Therefore, the grating is the first component to be selected, as it is the most critical of all for a high quality setup.

Following the grating, a lens or spherical mirror with a specific focal length has to be chosen. Achromatic lenses, which reduce chromatic aberration, and antireflection coatings for higher transmission rates are preferred. Spherical mirrors should have gold or silver coatings for a higher reflectivity.

To find suitable focal lengths for the lenses or mirrors, a program was written to calculate the incident angle fitting the parameters focal length, spectral width and LCM width, as these parameters define the deviation in the angles for the two wavelenghts. Figure 4.2 shows how the different design parameters are connected to each other geometrically. The angle, which the lowest wavelength of the spectrum is diffracted to, can be calculated as

$$\beta_l - \beta_m = \arctan(\frac{w_l}{f}), \tag{4.1}$$

with $w = w_l + w_h$ as the width of the spectrum. Calculating the deviation of the two angles, $\beta_l - \beta_h$, a common incident angle for both can be found. Ideally, a near-Littrow configuration is used, which can be found by trying different focal lengths available from the optic manufacturers. The tuning parameter to find a Littrow angle is usually the spectral width, for which small variations from the desired width can be made to find a configuration with off-the-shelf components. Also, the width of individual pixels has to be considered, as all the same frequencies in the beam form

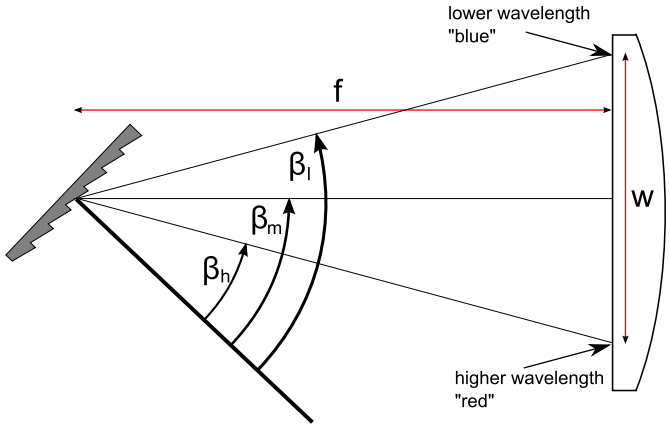

Figure 4.2: Connection of important design parameters

a new beam of the same size at the focusing element (see figure 4.4). At the focal point, in the Fourier plane, this beam experiences its minimum diameter, whereas its width should not exceed the width of a single pixel of the SLM. Using the lens equation (2.21) and the specifications of the SLM, a minimum beam diameter can be calculated. If the beam diameter in the setup was smaller, a bigger spot on the SLM pixel would result in leakage of frequency components to more than one pixel.

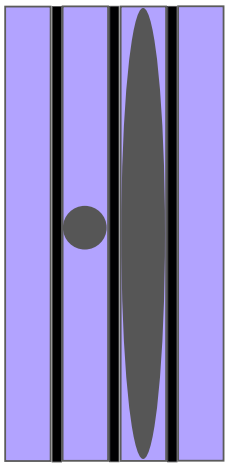

Figure 4.3: Focusing in only one dimension allows a lower intensity on the crystals

For higher power applications, the damage threshold of the SLM needs to be considered as well. The wider models with a greater number of pixels do not only offer higher resolution, but also a greater area, allowing to divide the total pulse energy on a larger area and therefore a lower intensity. Using the whole area is not trivial, as most pixels are taller than wide (in case of the used SLM, the ratio is about 50:1), the spectral components should only focus in the horizontal direction (see figure 4.3). Therefore, cylindrical lenses or mirrors should be used when the intensity of the laser is critical. Usually there is a tradeoff, as cylindrical lenses are more widely available, but increase optical errors for shorter pulses, whereas cylindrical mirrors are often not available in the required sizes. It may also become necessary to increase the size of the beam to match the height of the pixels and then redesign the other components so that the focused width also fits the size of one pixel.

If the gratings are not used in a Littrow configuration, the influence of the different angles on the beam diameter also needs to be included (figure 4.4) Here, a larger angle away from the grating normal results

in a smaller beam diameter.

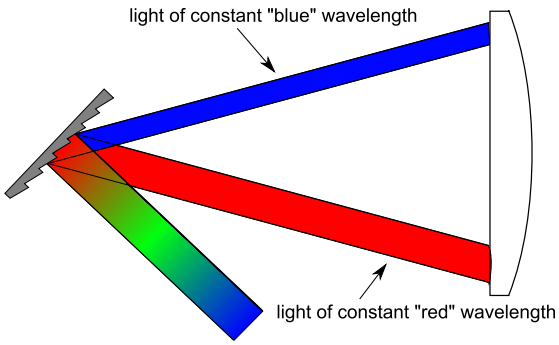

Figure 4.4: Width of spectral components of equal wavelength on the focusing element

4.2 Characteristics of the SLM device

The SLM used in this project is a CRi SLM-640-D-VN[2] model. It has 640 pixels in two masks for separate phase and amplitude modulation. Its dimensions are $64x5mm$, whereas each pixel has a width of $100\mu m$ and an interpixel gap of $2\mu m$. It's polarizers are optimized for a wavelength range of 488 to $900nm$. The losses are given by $P_L < 6\%$, plus coating losses of $P_{L,coat} < 3\%$ and polarizer losses of $P_{L,Pol} \approx 25\%$, leading to an overall transmission of $\frac{P_{out}}{P_{in}} \approx 68\%$. Its pulse damage threshold is given with $200\frac{\mu J}{cm^2}$ at $890nm$ for a $50fs$ pulse at a repetition rate of $1kHz$. The pixels can be adressed with a voltage from 0 to $10V$ in a 12 bit resolution.

4.3 Lens setup

The first setup that was built used two lenses. All optical components were aligned along an optical axis (compare to 3.1). Table 4.1 shows the components used.

For the axis, optical rails were used, on which the components could easily be translated in one dimension. The two gratings were each positioned on a rotational mount, a vertical post and a gimbal prism mount, which allows to position the grating at the rotation center of the mount. A precise alignment concerning the distances between grating and lenses can be achieved by using this rotation center, where the beam impinges on the grating. The whole setup, mainly due to the rail, is higher than the input

[2]http://www.cri-inc.com/products/components.asp

Component	Part number	Technical data
Diffraction grating	Thorlabs GH13-18V	holographic reflective, visible light, $(12.7mm)^2$, $G = 1800\frac{1}{mm}$
Lens	Thorlabs LA1353	d=75mm, f = 200mm, singlet, no AR coating
Beam steerer	Newport 670-RCT	Vertical beam translator
Mirrors	Newport 10B20UF.25	Ultrafast 45° Dielectric broadband mirror
Polarization rotator	Newport PR-950	700-1200 nm, 10mm clear aperture

Table 4.1: Components used for the lens setup

beam, so a vertical beam steerer was used to translate its height. After the calculation of the angles for the grating, the center wavelength at angle β_m (see figure 4.2) is directed onto the optical axis. The incident beam before the grating is reflected by a mirror, which is placed at a position determined by the input angle. Therefore, this mirror should be as far away from the grating as possible to reduce geometrical errors, since small errors from the positioning of the mirror cause relatively large errors for the incident angle, which should be accurate to within $\pm 0.5°$, if possible, to make sure the calculated spectrum size on the SLM does not differ too much from the real spectrum. A mark on the grating mount and the holes on the optical table served to measure the distances necessary to place the mirror in its appropriate position. If the incident light does not diffract perfectly onto the optical axis, small adjustments of the rotational mount angle can be made. At an input angle of 29.5°, the shorter cut-off wavelength of $775nm$ is diffracted to 64.6° and the longer wavelength of $825nm$ is diffracted to 82.8°, respectively.

The second grating was mounted on a similar device as the first one, but has a precision translation stage to make sure the 4f-condition is met. The calibration procedure is done without the SLM present, and the geometric calibration makes sure that the pulse is not broadened after leaving the setup. The SLM calibration itself follows, but none of the other components are changed at this point.

Initially, power measurements showed that the output beam was very weak. The reason for that was a change in the polarization of the laser due to a Faraday rotator, which was used to prevent damage from light reflected back into the laser. The gratings, however, are polarization dependent. The efficiency curve for the used grating is shown in figure 4.7. It is obvious that for the center wavelength of $800nm$ the efficiency is highest in the S-plane, which is the horizontal polarization. Therefore, a polarization

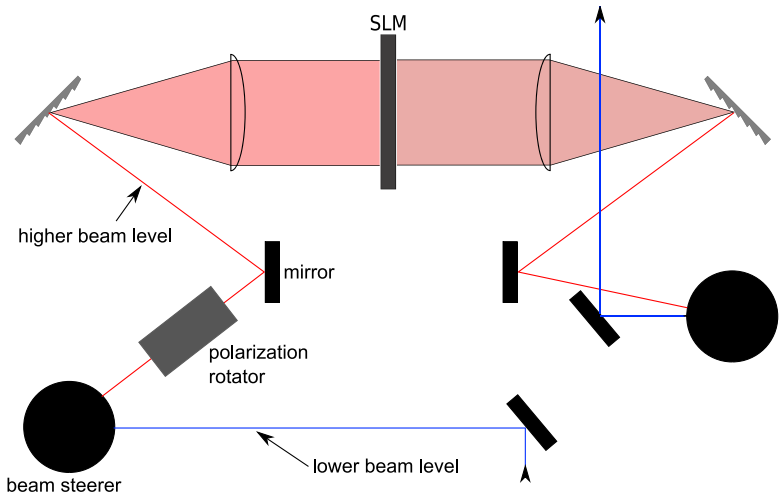

Figure 4.5: Drawing of the setup with lenses along an optical axis

rotator had to be inserted to maximize the output power after the second grating.

Initially, the beam was diverging too much after the setup, which made it almost impossible to perform a FROG measurement to characterize the temporal properties of the pulse. Two plano-convex lenses separated by two focal lengths, which, if one lens is moved a little bit off focus, can collimate the beam, were used to improve the results. It is necessary to have a collimated beam at the input, as the two lenses in the pulse shaper cannot be used to compensate for this effect. The pulses could be measured despite the low power and poor collimation. Nevertheless, the setup was far from being optimized and the calibration never returned the proper results. Therefore, we decided to change to a setup with reflective optics.

4.4 Spherical mirror setup

As mentioned earlier, reflective optics are preferred for ultrafast pulses as they reduce dispersive effects. Additionally, a reflective setup is, in general, more compact than a lens setup, since folding mirrors can be used which allows for a reduction in the total length of a pulse shaper by at least a factor of 2 compared to a 4f lens setup as shown in figure 3.1. As space issues are especially a problem for our wider, 640 pixel SLM, which requires longer focal lengths, a reflective setup became necessary. Spherical mirrors with a more than double focal length compared to the lens setup were chosen, which allowed a higher flexibility and over all, better performance. The setup can be used in a Littrow configuration, increasing total power throughput and allowing for an

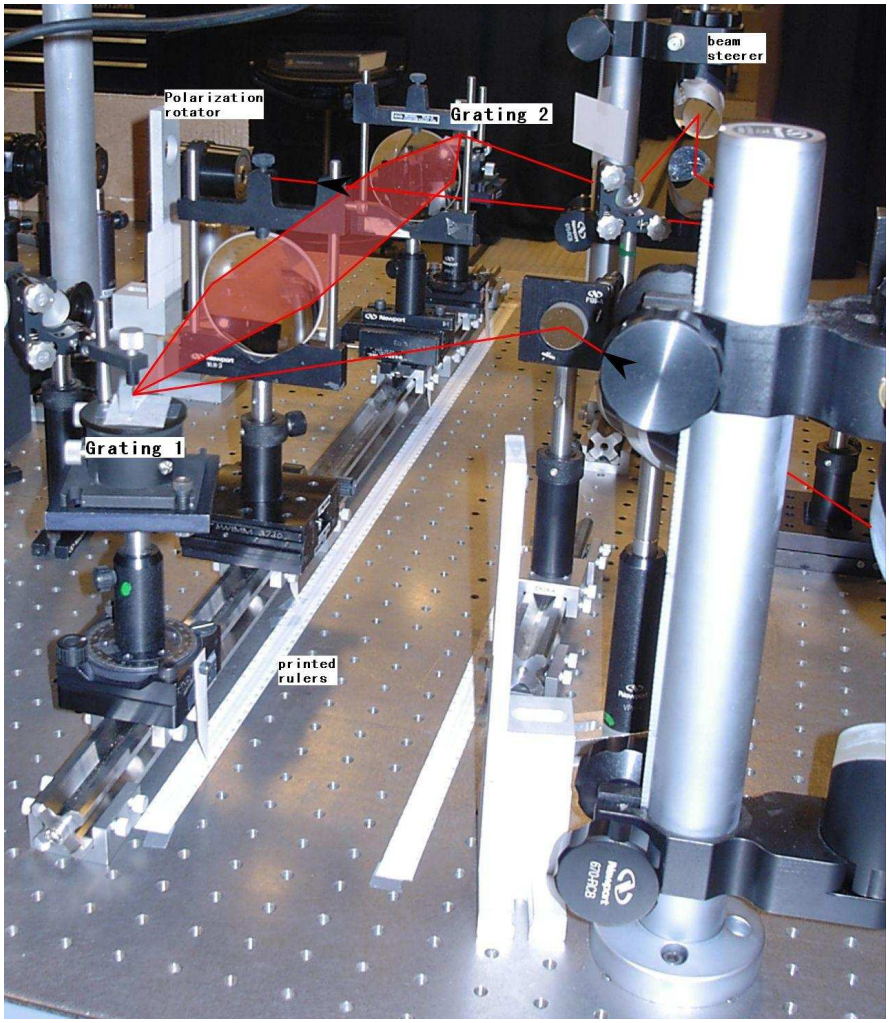

Figure 4.6: Picture of the setup with one optical axis. The beam path is highlighted in red for a better illustration.

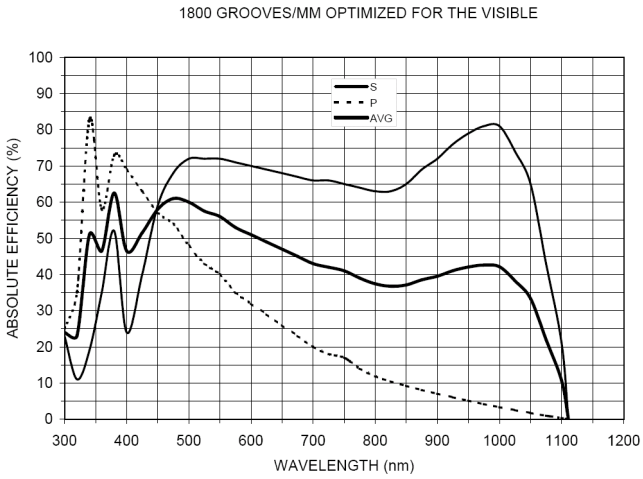

Figure 4.7: Efficiency curve for gratings Thorlabs GH13-18V [Tho07]

easier alignment of the input angle. The design according to figure 3.4 was chosen over the setup depicted in figure 3.6 because of the larger size of the spherical mirrors, which was required by the wide active width of the SLM compared to the proposed setup in [PWA03]. Due to the large diameter of the spherical mirrors, large tilting angles for the grating and mirror would have been required with a subsequent increase in optical errors. A possible solution is, as the spectrum on the spherical mirror only spreads horizontally across the center axis, to cut a hole in the spherical mirror. This would allow us to send the input beam closely above the diffracted spectrum into the setup and decrease the required tilting angles of grating and mirror (figure 4.8). Cutting a mirror is permanently and makes them not usable for other purposes. This procedure is therefore only recommended for space-critical applications, however, it provides the possibility to use very long focal lengths as well. An overview of the components is given in table 4.2.

The D-shaped mirrors (spherical mirrors cut in half) replaced conventional, round mirrors as folding mirrors because of their ability to keep the input beam and the diffracted beam close together, especially when spherical mirrors with $f = 20cm$ were used. The required tilting angles caused COMA, but the biggest problem was the vertical tilt of the spectrum in the Fourier plane. Although this is an inevitable systematic error, it can be minimized with the D-shaped or rectangular mirrors. An alignment procedure can be found in the appendix. The first measurements were taken with a $1800\frac{lines}{mm}$ grating, but later replaced with a $2000\frac{lines}{mm}$ grating. The first gratings allowed a Littrow configuration at 45° for both the input and the output angle, with a spectral width from 773 to 827 nm, and therefore a shorter width of the necessary parts of the spectrum.

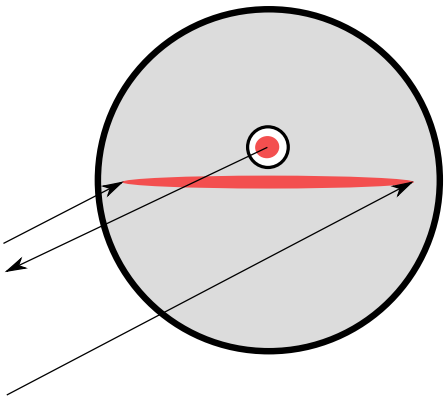

Figure 4.8: A hole in the mirror allows the beam to enter the setup at close proximity to the dispersed spectrum

Component	Part number	Technical data
Diffraction grating	Newport 10HG2000-475-1	holographic reflective, $(25mm)^2$, $G = 2000\frac{1}{mm}$
Spherical mirror	Edmund Optics NT32-831	d=76.2mm, f=457.2mm, Au coating
Folding mirrors	Thorlabs PDF10-03-M01	D-shaped mirror, $\frac{\lambda}{10}$-surface flatness, Au coating
Polarization rotator	Newport PR-950	700-1200 nm, 10mm clear aperture

Table 4.2: Components used for the spherical mirror setup

This could be solved by using the higher resolution gratings, where the spectrum is spread from 779 to 821nm at an angle of 53°, resulting in a higher resolution for the pulse shaper. This shows the necessity of carefully choosing the components for each different laser source.

The width of the spectral components at the SLM was calculated to be 397μm for a beam radius $w_0 = 1.2mm$ and a wavelength $\lambda = 820nm$. This is 4 times higher than the width of a pixel. When the SLM is used and only one pixel is switched to its dark state, the decrease in intensity for the corresponding wavelength is only very weak, which shows that each frequency component is spread over several pixels and then transmitted as well, although some of its central peak power is reduced. For this, a beam diameter of 1.2mm and the highest available wavelength component of 820nm has been used. Therefore, a larger beam diameter is necessary. A magnification of at

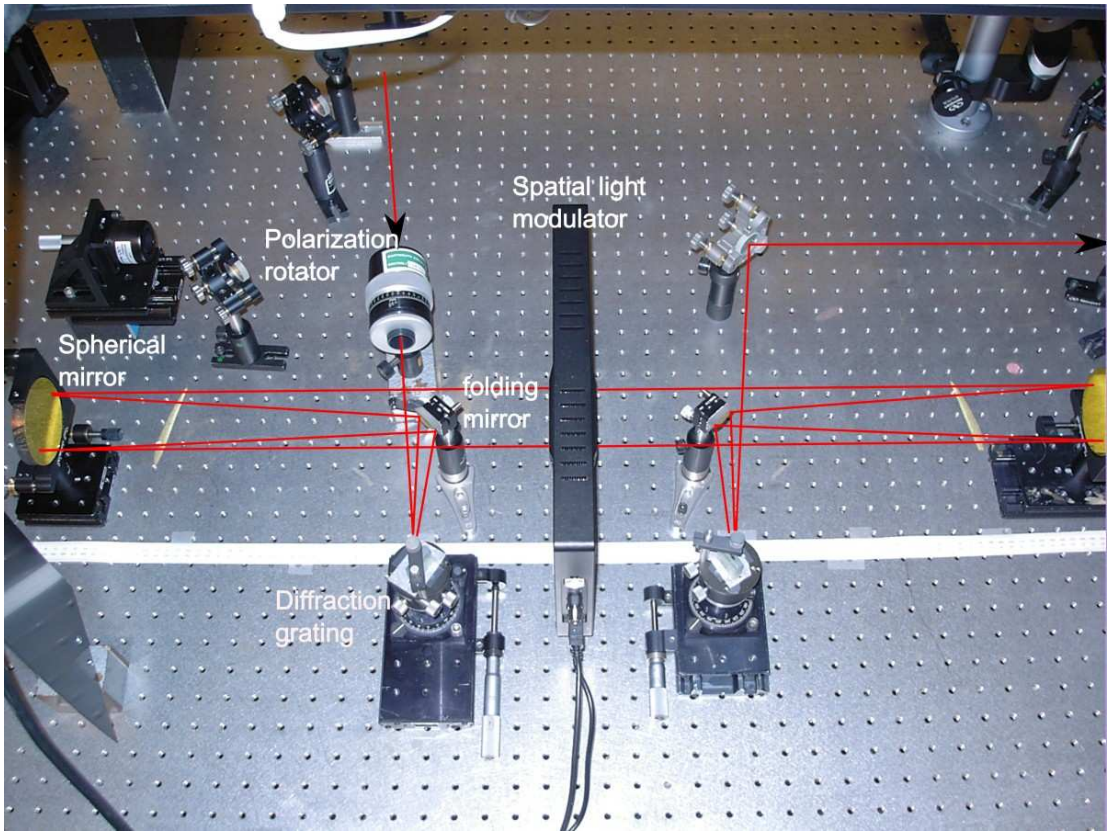

Figure 4.9: Picture of the setup with spherical mirrors.

least a factor of 3, if the $\frac{1}{e^2}$-wavelengths are considered, is necessary. A larger magnification would be even better for suppressing the influence of wavelength components on neighboring pixels on the SLM. In the lab, a beam expander with a magnification of 3 was available and used to check if the results were any better. The alignment of the setup becomes more difficult, as the bigger beam diameter requires a larger separation between the incoming beam and the folding mirror, resulting in a spectral tilt in the Fourier Plane. As the active area of the SLM is large enough, all spectral components still pass through the crystal array. However, the quality of the reassembled beam is not as good as the one with a smaller beam diameter. Therefore, the input angle was changed to a slightly smaller angle than the dispersed spectrum, so that it could pass next to the folding mirror on the same height. The grating did not need to be tilted then which improved beam quality again.

The damage threshold of the SLM also had to be considered. An average energy at the input of the SLM of about $500mW$ at a repetition rate of $80MHz$ leads to an energy of $6.25nJ$ per pulse. Focused to a height of $100\mu m$ and spread to a width of $64mm$, this equals a fluence of $97\frac{nJ}{cm^2}$, which is far below the damage threshold. With the MaiTai-laser, the SLM can be used without fear of destroying it. For more powerful lasers, however, this value has to be recalculated.

4.5 Upgrading for other laser systems

As the laser source is exchanged, the setup usually has to be reconfigured. Most importantly is the width of the pulse, where a shorter pulse relates to a broader spectrum due to the uncertainity principle. A broader spectrum can be diffracted wider, which results in either a shorter distance or a grating with a lower groove frequency, which makes the choice of the components, in general, easier.
A second laser system was available, which contains a SpectraPhysics Tsunami, a Ti:Sapphire laser pumped by a solid-state laser, generating pulses at a width of shorter than 100 fs at a repetition rate of 80 MHz. This beam is then sent through a Spitfire Pro® amplifying system, which reduces the repetition rate to 1 kHz, resulting in a much higher pulse energy and a pulse width of about 35 fs at a beam diameter of $12mm$ at the $\frac{1}{e^2}$ points. Not only the broader spectrum has to be considered, but especially the larger power can cause problems due to the damage threshold of the SLM. Also, the bigger beam diameter implies a smaller focused beam, if dimensions are not changed.

To solve the power problem, the standard focusing components can no longer be used. Instead, as mentioned earlier, focusing in only one dimension is a solution. Lenses are no longer suitable for the short width of the pulse. Therefore, cylindrical mirrors need to be used. They are now the first components to choose, as choices are very limited for cylindrical mirrors. As cylindrical mirrors from the standard suppliers have not been available in the required sizes for this pulse shaper, only a few general considerations are given. The general rules for choosing the components remain unchanged.
Considering a beam diameter of $5mm$, which is the maximum for the height of the SLM, a wavelength of $850nm$ and a focused width of $100\mu m$, the lens equation returns a necessary focal length of $f = 462mm$. The illuminated area of the crystals is $A = 0.64cm^2$. Therefore, in order not to exceed the damage threshold of $200\frac{\mu J}{cm^2}$, the pulse energy should not exceed $128\mu J$, which is below the output energy of the laser amplifier. The grating threshold can be a problem, as it is lower for S polarization, which is used here. Also, the coating is essential. Holographic gratings with an Aluminum coating have a threshold of around 0.1 $\frac{J}{cm^2}$, whereas gold coatings increase this value by an order of magnitude to around 1 $\frac{J}{cm^2}$ [PaL05].

Chapter 5

Program control

As an electronic device, the Liquid Crystal Modulator is fully controllable with either a control program able to load predefined patterns with values for each individual pixel or with high-level drivers for Matlab®[1] or LabVIEW™[2]. LabVIEW was preferred because it offers drivers for most equipment in the lab (such as spectrometers or power meters) and can therefore integrate parameters for an automated feedback design. Also, it is able to use Matlab scripts, when simple and fast manipulation of data is required. LabVIEW is a graphical programming language in which devices can be placed and connected with elements from a virtual instrument screen, the Front Panel, where buttons, controls and graphs can be displayed. Data can be aquired, processed and sent back to the device.

5.1 Labview program

The driver for the SLM comes with different Labview programs. These so-called Sub VI's can be used in a larger program and provide basic low-level functions to adapt the SLM to individual applications. They include the following functions:

- Initialize: Returns important data from the SLM device such as number of pixels or number of masks
- Mask Select: Chooses which mask (in a dual mask system) should be used to write the frame pattern to
- Define Pixel: Sets a pixel in the selected frame to a defined drive value
- Read Pixel: Returns pixel drive value

[1] http://www.mathworks.com/products/matlab/
[2] http://www.labview.com/labview/

- Save Frame: Writes a whole array of values for all pixels into the selected frame
- Read Frame: Returns the array values
- Select Frame: Changes the currently used frame
- Cycle: Changes the active frame to the next available frame

which are all necessary for enabling all of the SLM functions.

The functionality of the Pulse Shaper should include the capability of reading defined patterns, but especially the definition of a desired output waveform was necessary. Also, the potential to include a feedback design was desired. The program was therefore structured into a main control panel and two SubVIs for calibration purposes.

5.1.1 Control panel

The control panel should include all functions necessary to use the pulse shaper. The flowchart on figure 5.1 shows its main functionality.

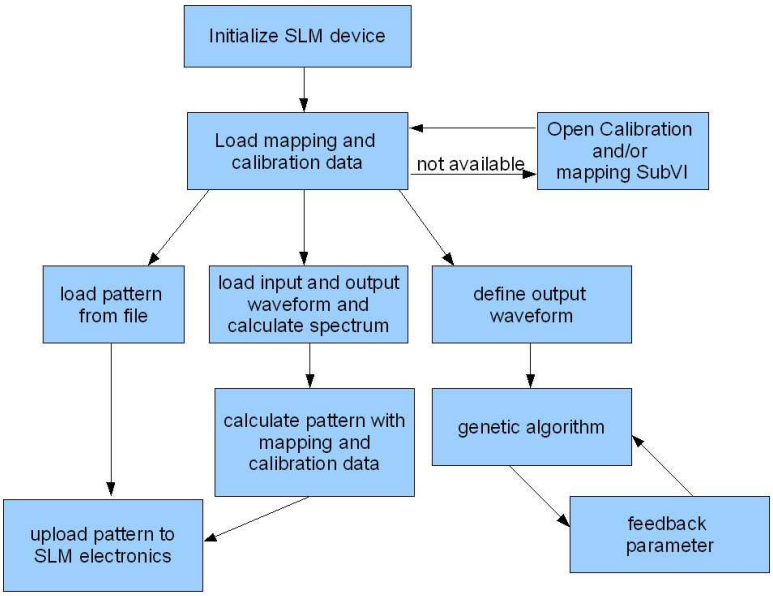

Figure 5.1: Flowchart of the SLM control program

Loading a pattern is essential for testing the main functionality and it can also be important if a particular pattern is known and has to be uploaded. The definition of the output pulse is the most useful function, if the pulse shape required by an application is known. Therefore, the time domain data, which is a measurement taken before the pulse shaper for the input pulse, and a defined output pulse, given in a text-file format, are read into the program. Using a Matlab script, the FFT is calculated. As the spectrum is centered around zero, it is shifted by the center wavelength of the input pulse, which has to be entered by the user. A zero-padding procedure is used to increase the number of datapoints of the spectrum, and the interesting spectral parts in a user-defined range are extracted for further calculations. Theoretically, a division of the output spectrum by the input spectrum yields the transfer function for amplitude and space, as described in section 3.1. Practically, if both functions are normalized to 1, a larger spectral amplitude value of some components of the output pulse would require a gain, which the pulse shaper cannot provide. Picture 5.2 shows the influence of not adapting the whole desired waveform. Parts of the spectrum might be modulated as desired, but others are not, and the whole pulse becomes distorted. A better solution is to modify the waveform in the calculations beforehand, which requires wasting energy of attenuated components. Nevertheless it maintains the shape of the outgoing waveform. This is implemented by attenuating the whole waveform, so that the output spectrum contains no higher amplitude value than its equivalent in the input spectrum.

Then, the calibration values, where a specific wavelength is mapped to each pixel, are

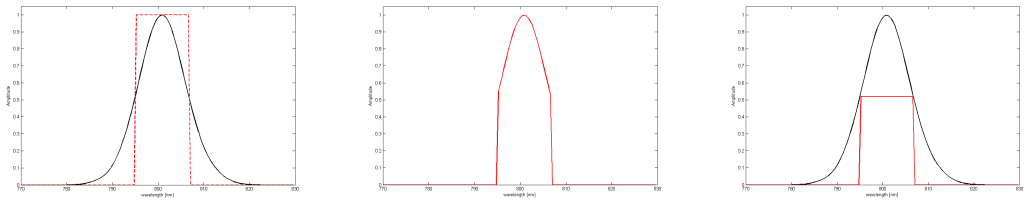

(a) (b) (c)

Figure 5.2: Effects of normalization to the available spectral amplitudes. **a** Available spectrum (black) with desired spectral waveform (dashed red). **b** Without normalization, maximum power, but desired waveform is falsified. **c** Attenuated amplitude allows to shape desired waveform

used to find the wavelengths in the input and output spectrum array that are closest to each pixel value. An interpolation could also be used for a higher accuracy, but does not seem to be necessary. The input and output values yield a transmission and phase value for each pixel on the SLM (see 1). Using the SLM calibration values (see

subsection 5.1.3), a drive value is stored for the amplitude and for the phase mask, respectively.

Algorithm 1 Pattern calculation algorithm for waveform shaping

1: **for** $i = 1$ to number of pixels **do**
2: calculate index j for which input_wavelength(j) is closest to pixel_wavelength(i)
3: calculate index k for which output_wavelength(j) is closest to pixel_wavelength(i)
4: Transmission(i) = Output_amplitude(j) / Input_amplitude(k)
5: Phase(i) = Output_phase(j) - Input_phase(k)
6: **end for**

5.1.2 Mapping tool

In order to precisely assign wavelengths to pixel values after the setup of the SLM, a mapping calibration needs to be carried out. Using an idea found in [Hof06], a single pixel is switched to active state and a dip is visible in the output spectrum, as the corresponding frequency component is blocked. Measuring the wavelength of the amplitude dip for several pixel values and interpolating between those values with a linear or polynomial function, a precise calibration can be made which can be used for all measurements, as long as the optical components are not moved away from their original position. The resulting mapping can therefore be stored in a file, which can be loaded directly in the control program.
A slightly different approach would be to switch only one pixel to the transmission state, such that the assembled beam consists only of one sharp frequency peak. This has the advantage that the calibration process could be automated if the spectrum is taken and loaded into LabVIEW automatically. Finding the peak in the data returns the wavelength of the pixel that was set to transmission. However, we found that the energy, especially of the sidebands, was too weak to allow a calibration with this procedure. Figure 5.3 shows two measured spectra with both techniques. It is obvious that the dip is much clearer than the single peak. Moving closer to a sideband makes this even more dramatic and a calibration becomes impossible.

Figure 5.4 shows a measured mapping file. As obvious, the curve is only slightly nonlinear and a quadratic polynom was sufficient to interpolate between the different values.

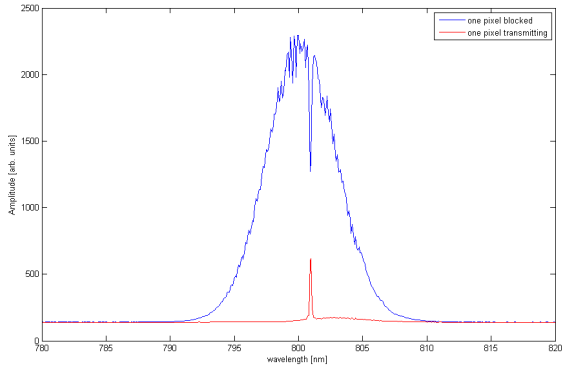

Figure 5.3: Comparison of two different mapping procedures, where one pixel (in this case pixel 320) was switched either to transmitting or blocking state. The reflective setup was used with a 3x-beam expander.

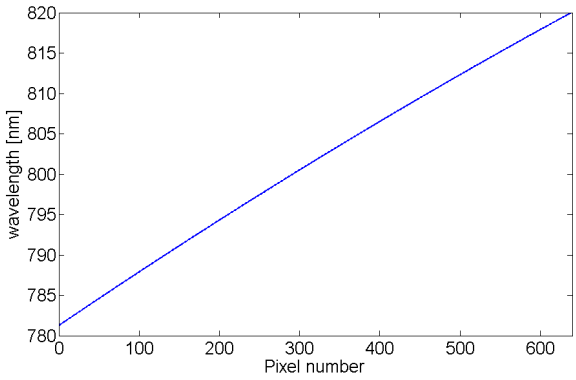

Figure 5.4: Measured pixel to wavelength mapping in the reflective pulse shaper setup.

5.1.3 SLM response calibration tool

The phase change for an applied voltage drive value is nonlinear and given by the supplier of the SLM. For our device, a graph is given in figure 5.5, which could be used for simple purposes. However, if more precise values are required, a SLM specific calibration table is recommended. Therefore, a tool was developed which automated the calibration process by integrating a power meter into the LabVIEW enviroment. Figure 5.6 shows the setup in the lab.

The program first sets one mask to its maximum drive value, which equals approximately a phase change of zero and full transmission. Then, the other mask is calibrated

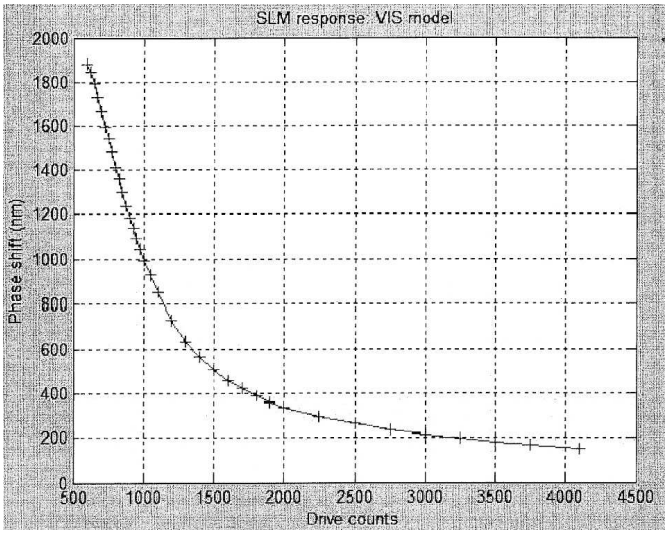

Figure 5.5: SLM response function from the manual [Cam04]

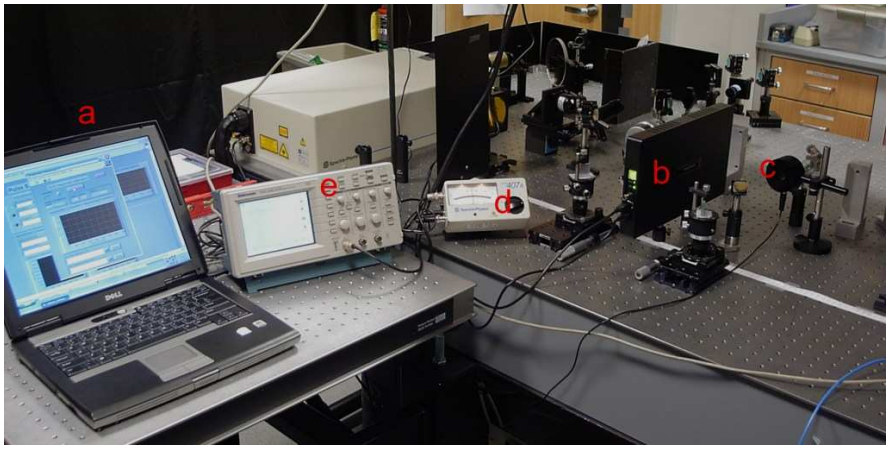

Figure 5.6: Automated calibration setup. A notebook computer **a** sends a drive value to the SLM **b**, and the output power of the assembled beam is measured with a power meter **c**. The analog output of the power meter **d** is measured through an oscilloscope **e**, which is integrated into the LabVIEW program on the computer.

by increasing the drive value from zero to maximum in equally spaced steps. The transmission value is recorded by measuring the output beam with a power meter. Using equations 3.5 and 3.6, the phase for the individual arrays can be calculated as

$$\Delta\Phi_1 = \frac{\pi}{2} + \varphi + \arccos(\sqrt{T}) \tag{5.1}$$

$$\Delta\Phi_2 = \frac{\pi}{2} + \varphi - \arccos(\sqrt{T}), \tag{5.2}$$

where $\frac{\pi}{2}$ needs to be added to avoid a negative phase retardance [Lup04]. Since the

transmission is "oscillating", that means it has several minima and maxima, the function needs to be regarded as a steady function, in order to have the phase retardance continously falling, since all multiples of 2π added to the phase retardance result in the same transmission value. This was solved by using an algorithm to change the sign of the $\arccos(\sqrt{T})$ term, when maximum transmission was reached, for recalculation of the phase retardance.

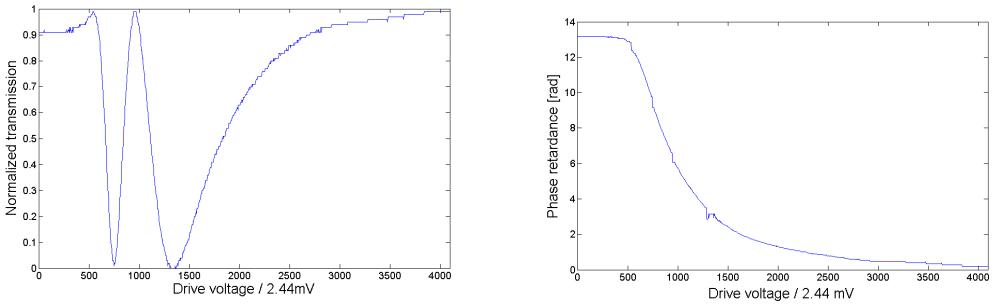

(a) (b)

Figure 5.7: Transmission values and the calculated phase retardance of one mask with a calibration procedure with 1024 steps.

5.2 Feedback with a genetic algorithm

A feedback implementation for the pulse shaper was developed to demonstrate the capabilities of a feedback design and to see how it can be integrated into the program code. First, a suitable feedback parameter was required, and a FROG measurement could not satisfy the needs of such a design, as a measurement takes far too long (about 15 minutes per single measurement) and often needs to be recalibrated. One option for the future could be a faster device, such as the Grenouille[3] FROG system, which provides real-time measurements. We decided on a Spectrometer which is used for the optimization of the spectral amplitude. This is related to the output pulse, but as the phase is missing, the pulse is not completely characterized. However, it can be used for certain purposes where only the amplitude of the pulse is required.
The Spectrometer is an OceanOptics HR2000[4], which provides a high resolution of $0.035nm$ FWHM. It is connected to the PC via a USB connector and drivers for LabVIEW are provided, which makes it easy to integrate it into the control program. First, a data structure for the chromosomes had to be chosen. As a genetic algorithm

[3]http://www.swampoptics.com/products_grenoverview.htm
[4]http://www.oceanoptics.com/products/hr2000.asp

works with binary variables, a long vector of bit values was used which contains 12 bits as a drive voltage for each pixel, altogether 640 pixels, and this for both masks in the SLM. This adds up to a total of 15360 bits for each chromosome. Together with the whole population of one generation this was stored in a matrix as shown in figure 5.8.

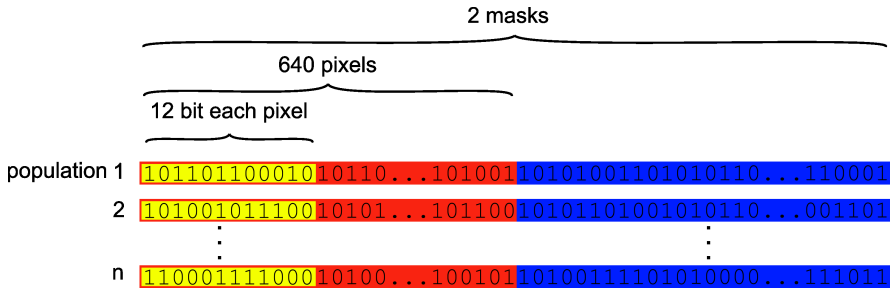

Figure 5.8: Data structure for the chromosomes of the genetic algorithm. Each pattern is stored in one array, and each chromosome forms one line of a matrix, which stores one population.

The start solutions were uploaded to the SLM, and a spectrometer measures the spectrum. The spectrum needs to be processed, as it has constant background noise added, which needs to be substracted. Then, the fitness function was applied and a fitness value calculated. Through the steps of selection, crossover and mutation, a new generation was created. The fitness factors were recorded and shown on a graph, so that the progress was visible.
After starting with random values, we implemented a function to load a calculated pattern that is already close to the right solution. This solution in general has a high fitness factor, and if it is implemented correctly, can serve to find an optimum solution much faster. If only these values were taken as a first generation, however, the algorithm might stop in a minimum which it could not escape from. The diversity of start solutions is important to find the optimum solution faster.

Algorithm 2 Genetic algorithm with feedback parameter

```
1: Calculate random first generation
2: while Fitness factor < Required accuracy do
3:    for i = 1 to size of population do
4:       Upload new chromosome to the SLM and measure feedback
5:    end for
6:    Evaluate solutions with a fitness function
7:    Select a new generation by weighted fitness
8:    Select solutions for crossover according to P_cross
9:    Crossover
10:   Mutation according to P_mut
11: end while
```

Chapter 6

Experimental results

In order to show the capability of the pulse shaper to generate arbitrarily shaped pulses, some examples, representing different applications, have been performed.

6.1 Spectral shaping of a rect function

For testing of the spectral shaping program, a rectangular function was chosen to be shaped, since it is a comparatively easy waveform. Spectral shaping can be interesting when information is transmitted in the spectrum of the pulse, such as in optical communication.
The program requires to measure a spectrum beforehand, and to define a desired output waveform based on the same wavelength vector as the measured spectrum. It then uses the calibration and mapping values to calculate the pattern for the two masks of the SLM. First, a spectrum was used that was measured without the SLM inserted. Figure 6.1 shows the result. It is obvious that the output waveform has approximately the same sharp sidebands as the desired rect function, but the amplitude is not uniform, which is due to effects of the SLM, such as pixelation or interpixel gaps. Also, the total number of measurement points for the amplitude is less than the number of SLM pixels, since the spectrum is very narrow. Therefore, a precise mapping is not possible, instead, an interpolation procedure should be used.

Additionally, we tried to improve the results by using the spectrum measured after the SLM as an input function for the program. As one can see, the results are not much better, but the average of the values seems to be more uniform than in the first measurement.

The patterns with the pixel voltage drive values look similar (figure 6.3). The second pattern is a little "noisier", as it tries to compensate for the input spectrum. Also obvious is that since the spectral modulation is a pure Amplitude modulation, some drive values are zero, which means a large phase shift that is neglected here.

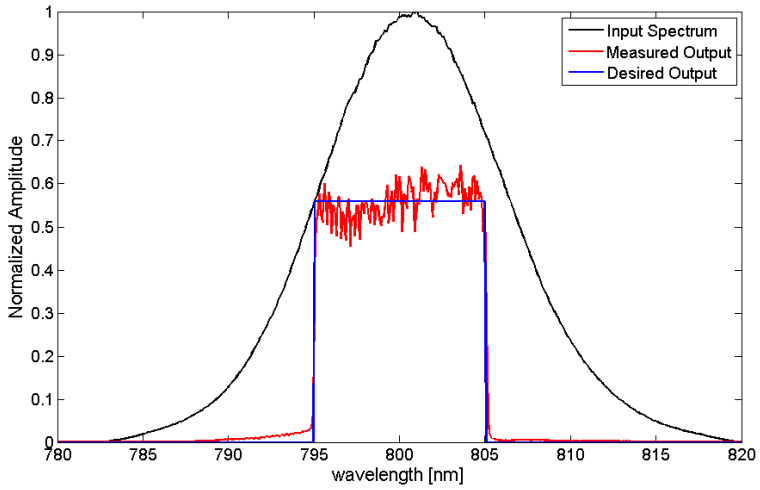

Figure 6.1: Shaping of a rect function in the spectral domain. The input spectrum is a Gaussian (black) measured without the SLM inserted. The output (red) varies from the desired spectrum (blue) due to errors introduced by the SLM.

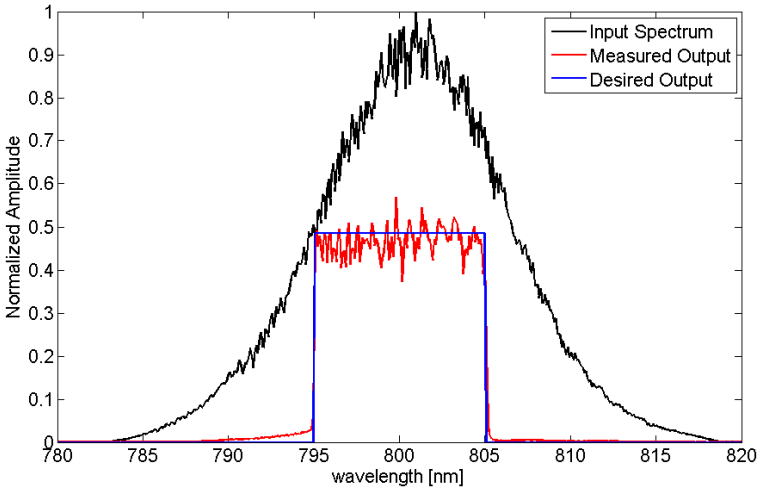

Figure 6.2: A modified input spectrum, measured with the SLM inserted, does not significantly improve the results.

6.2 Feedback shaping

The feedback shaping program was designed to allow to start either with a start solution or with completely random solutions. When a start solution was chosen, the spectral shaping procedure needs to be used beforehand to calculate a SLM pattern

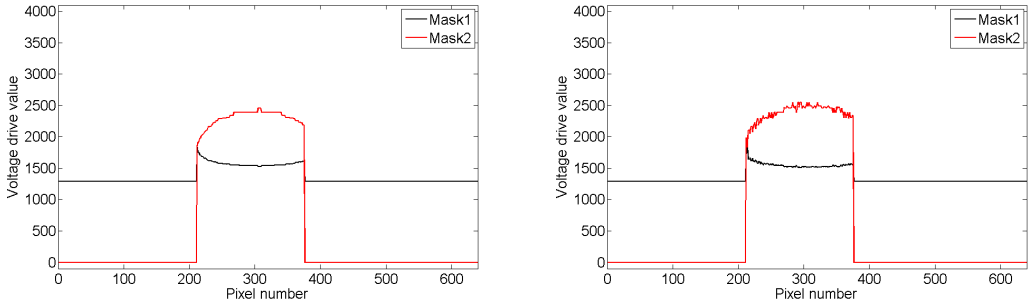

(a) Spectrum without SLM

(b) Spectrum with SLM

Figure 6.3: Voltage drive values for both input spectra.

from theory. This is stored in a file and can be read in the feedback program. Then, it serves as the first solution to use for the first generation, the rest of the population is created as a random bit string. For the feedback, an algorithm calculates the difference between the measured and the desired spectrum in every pixel, squares these values and sums them up. This serves as a fitness factor, in this case, the lower the value, the better the function. Therefore, not the highest fitness value, but the lowest was to be looked for. The probabilites are calculated for each chromosome with the fitness factor, but then inverted, so that lower fitness factors receive a higher chance of being selected. After a renormalization of the probabilites, the algorithm was started. By the time of several generations, the one start solution dominated the selection process. The fitness factors finally varied between two values (see figure 6.4), which is supposed to be a storing error in the program. A better pulse shape than the calculated one was not obtained. This was maybe also due to another problem, that both arrays, measurement and desired spectrum, have been normalized.

Since the maximum value is one, only a few single peaks cause the average spectrum to be much lower than the desired spectrum, and the function can not approach the optimum from both sides. This is believed to be the major problem for the algorithm. Absolute values are not suitable to be taken, however, it might be possible to normalize the measured spectrum to an average value in the interesting area.

6.3 Shaping in time domain

For shaping in time domain, a FROG measurement of the input pulse was taken. The idea was to define a pattern that was able to shape the amplitude in time, and the phase

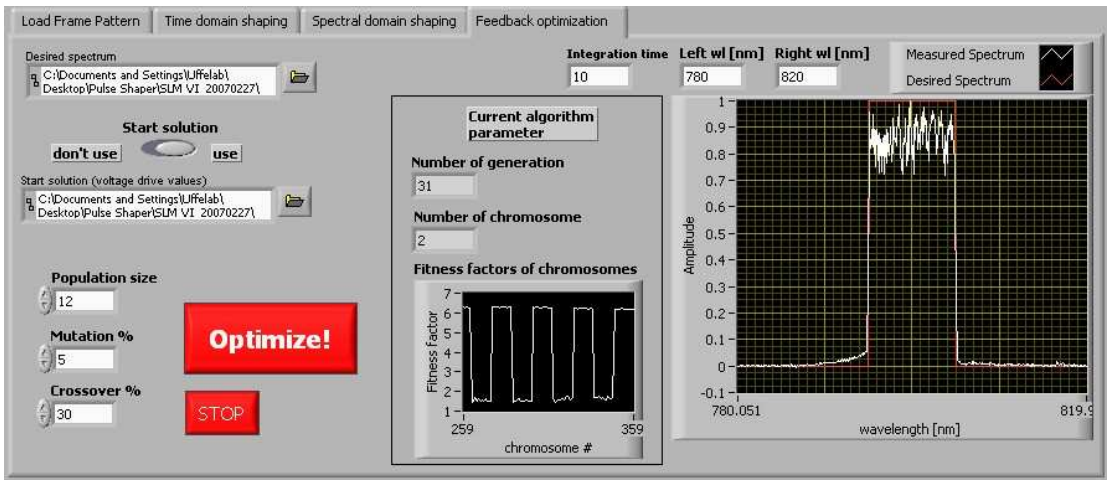

Figure 6.4: Feedback shaping with a start solution. The initially calculated solution has not been improved.

retardation through the pulse shaper should remain zero. For the output pulse, the time base of the input was used to create a rectangular shaped pulse and stored as a file. The input pulse can be seen in figure 6.5. Based on the rectangular pulse in time domain,

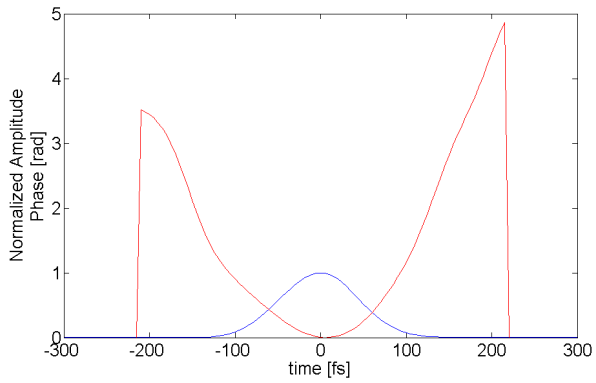

Figure 6.5: Input time domain data in amplitude (blue) and phase (red) as measured with a FROG device. The amplitude is normalized to 1.

a Fourier transform calculated a corresponding sinc function in frequency space. In order to use as much power as possible, only three sidelobes could be considered. The calculated spectrum is shown in figure 6.6. Using this function, the mapping procedure was applied to calculate the transmission values for each pixel. As the phase shift should remain zero, the phase function equals zero over all pixels. Finally, the SLM calibration values were mapped to the transmission values, and the patterns for the master and the slave mask of the SLM were calculated. They are shown in figure

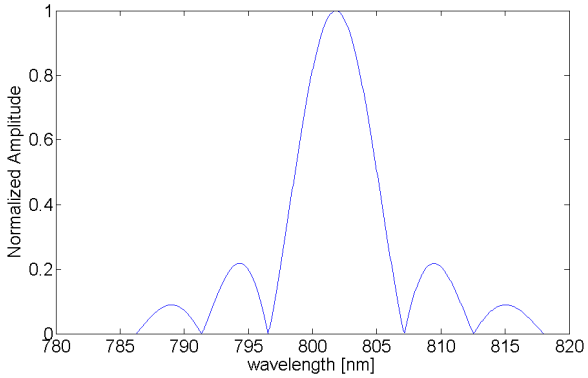

Figure 6.6: The sinc function is the frequency domain equivalent of a rect pulse in time domain. This function was used to calculate a pattern to shape a rect pulse in time domain.

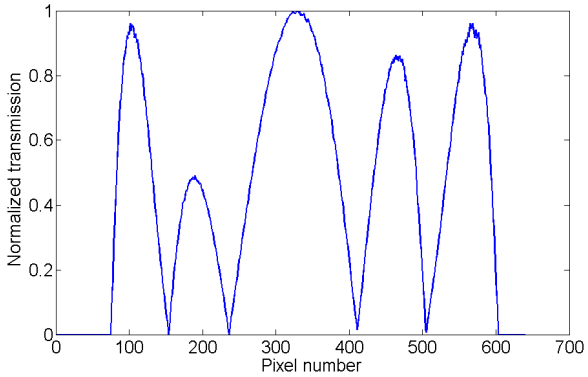

Figure 6.7: Normalized transmission values for the SLM to shape a sinc function.

6.8. The FROG measurement was a little more complicated. First, the reduced power caused problems when the peak of the second harmonic beam was searched for. Also, more data points became necessary due to the longer pulse width. When loaded into the FROG phase and amplitude retrieval program, a lot of datapoints were necessary to have a comparatively low error. As the results (figure 6.9) show, the desired time domain pulse could not be obtained. One of the possible reasons is the lack of higher frequency components, as only two sidelobes were considered. For a comparison, a superposition of a $sin(x)$ function and the two higher order harmonics, $sin(3x)$ and $sin(5x)$ is shown in figure 6.10. It is obvious that more frequency components are necessary to shape a rect in time. A shorter, broader input pulse is much better suitable for this purpose than the input used. Also, the error from the FROG program was not very low. It is doubtable that this shape has the least error, but since calculation

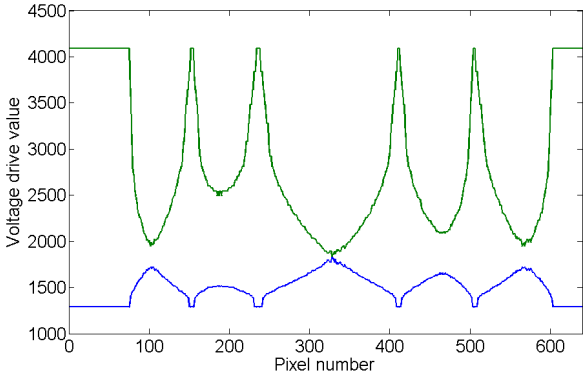

Figure 6.8: Voltage drive value pattern for the master mask (blue) and the slave mask (green) for a sinc function.

requires a lot of time for a complex pulse, the calculation had to be stopped some time.

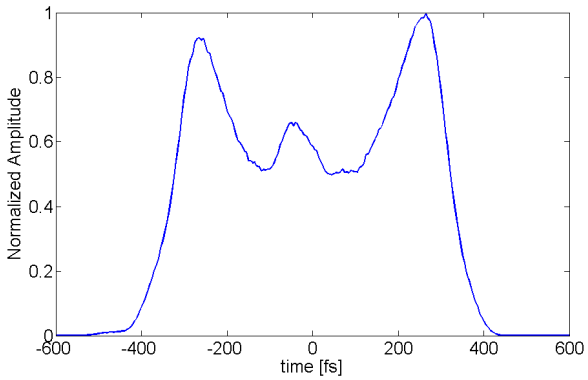

Figure 6.9: Measured amplitude of a desired rectangular function in time domain.

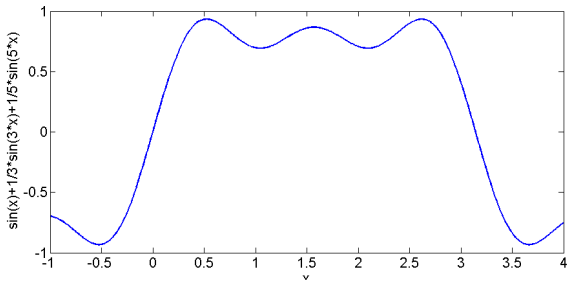

Figure 6.10: A superposition of only 3 frequency components does not result in a rect function. Therefore, more higher order components are necessary.

Chapter 7

Summary

In this work, an ultrafast pulse shaper based on a spatial light modulator was developed. A software for a flexible use based on the LabVIEW program has been created. Together with the hardware, the pulse shaper has proven to be capable of creating arbitrily shaped pulses, although a lot of considerations need to be taken if more complicated waveforms need to be shaped. An easy function in time domain is often much more complicated in frequency domain, where pulse shaping takes place. The fundamentals for a feedback design have been proposed and integrated into the setup. The algorithm has proven to work, but it certainly needs improvements for better results.

7.1 Improvements for the present pulse shaper

For the device built, several potential upgrades have been proposed in this work. On the side of the optical components, cylindrical mirrors or lenses would allow to use higher power lasers. A different setup could be used for more space critical applications. If a higher phase modulation is required, a reflective design as proposed would help. The software can be improved in the feedback design with the genetic algorithm. Here, more sophisticated techniques for evolutionary algorithms can help to obtain better results. Starting from easier implementations such as double crossover, which allows crossover within a chromosome, and a better evaluation function, and the experimentation with the parameters population size and the probabilites for mutation and crossover, more difficult topics can be tackled. One could be to find a normalization for the output spectrum that allows an average approach of the measured function towards the evaluation function, which is supposed to increase results significantly. Also, the coding of the parameters can be improved. Since the accuracy does not need to be perfect in the first place, one can start with a coding of 8 bits instead of 12 bits for the voltage drive values for the SLM. Also, an adaptive increase and decrease of

chromosome size is possible, which makes sure that the solutions approach the desired function quickly, and additional parameters then allow to increase the accuracy.

7.2 Future work

With a more reliable feedback implementation, a lot of different topics, such as optical communication or absorption experiments, can be investigated using a pulse shaper. Today, the approach towards understanding complex systems is often to understand simple concepts first and then build a model that describes the phenomena that have been observed. Pulse shaping, especially in the feedback implementation, can help to obtain new experimental data that has not been recorded before. Essential for the success of such an experiment is the knowledge about suitable feedback parameters. Some experiments certainly still have the prospects for further research, and systems like air or water do not necessarily need to be less complex than chemical experiments. Such systems may have some potential for experiments that could result in a better understanding of them.

A Appendix

A.1 Alignment procedure for a lens setup

The lens setup is easier to align than a reflective setup, as all components can be placed on one straight line and the beam height does not need to be changed. The following steps should be taken in order to have a functioning setup.

1. Place one mirror on the table. Redirect a laser beam from a calibration source (collimated beam, e.g. a HeNe-laser) through the mirror on a chosen height for the whole setup and adjust the height of the lens such that the beam travels parallel to the table before and after the lens.

2. Place a second mirror approximately two focal lengths from the first mirror and adjust its height for a parallel beam.

3. Observe the beam after the second mirror in the far field and change the mirror position, until the beam diameter is minimized. Then, the 2f-condition should be fulfilled and the outgoing beam is collimated.

4. Place the first grating one focal length before the first mirror and turn it to its calculated angle.

5. Position a steering mirror before the first grating to match the required input angle.

6. Place the second grating one focal length after the second lens and turn it to a symmetric position to the first grating.

7. Redirect the laser beam onto the steering mirror, which needs to be rotated to project the beam at the center of the first grating. Check the beam height before and after the steering mirror and make sure it is parallel to the optical table at its defined height.

8. Observe the dispersed and the reflected beam (order 0 and -1) of the grating tilt the grating iteratively for both beams traveling parallel to the table.

9. Observe the spectrum on the first lens and make sure it is centered by tuning the grating angle over a small range.

10. The spectrum should focus at the Fourier Plane and also be centered at the second lens.

11. Tilt the second grating for a parallel beam similarly to the first one.

12. The outgoing beam should be reassembled at the same angle as the beam impinges on the first grating. To make sure the angle is correct, the beam can be examined in the far field and a card can be sweeped through the dispersed components in the Fourier plane. If no spatial errors are present, the beam should be uniformly attentuated when some frequency components are blocked. Otherwise, an image of the card travels through the assembled beam. Optimize the result by precisely rotating the grating.

13. If the input beam does not have the polarization required by the gratings and the SLM, place a polarization rotator before the first grating and measure the power of the outgoing beam. Rotate the polarization plane to maximize output power. This should match the polarizer specifications of the SLM, as the setup was designed for a specific plane of polarization.

14. Measure the outgoing beam's characteristics with an ultrafast measurement method such as FROG. If the pulse is too broad, adjust the positions of the two gratings to make sure the 4f-condition is met. This is a critical parameter which requires high accuracy. A good way is to use precision translation mounts below the gratings, change their positions and compare the translation lengths with the width of the pulse.

A.2 Alignment procedure for a reflective setup

1. Place the mount for the SLM in the center of the setup.

2. Place both mirrors one focal length in front of and behind the now defined focal plane. A microtranslational mount is recommended for precise tuning of the 2f condition.

3. Position the folding mirrors about $\frac{1}{3}$ to $\frac{1}{4}$ from the focal plane. The first grating needs to be placed this distance from the folding mirror. In this way, the spectrum should not be broader than the folding mirror and no wavelengths are lost.

4. Use a steering mirror to direct the input beam close to the folding mirror and onto the grating.

5. Make sure the spectrum diffracts parallel to the optical table. Turn the grating so that it is centered on the folding mirror, which can be seen with an IR viewer.

6. The height of the folding mirror can be adjusted such that no spectral components are lost (a dip in upper region of the reflected spectrum). However, the height should not be unnecessary high to avoid large tilting angles.

7. Rotate the folding mirror so that the diffracted spectrum is centered on the spherical mirror. The height has to equal the height of the beam in the focal plane, which is also the height of the center of the spherical mirror.

8. Tilt the spherical mirror vertically to make sure that the spectrum is parallel to the optical table and on the correct height in the Fourier plane. Rotate it so that the spectrum is centered on the second mirror (IR viewer).

9. Tilt the second mirror such that the spectrum fits onto the second folding mirror.

10. Observe the diffracted spectrum from the second folding mirror and make sure it is parallel to the optical table and at the correct height. If not, adjust height by tilting the second spherical mirror and the folding mirror iteratively.

11. Place the second grating at its defined position and tilt it so the 0-order and 1-order beams are on their correct height and parallel to the table.

12. The outgoing angle should now be the same as the input angle, which means the distance from the beam to the folding mirror can be examined. Also, a card in the Fourier plane can be used to check for uniform attenuation like in the lens setup.

13. For the femtosecond alignment, vary the distance of the gratings to the folding mirrors and measure the beam in time domain until it is as short as it was entering the setup.

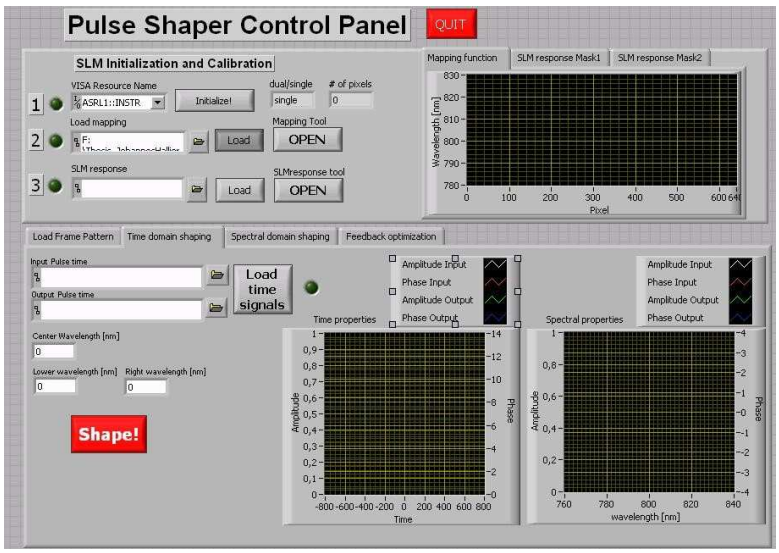

Figure A.1: Screenshot of the control program with the register for shaping of a time domain pulse opened.

A.3 Performance curves of used materials

A.4 Manual for the control program

1. Choose the device in the VISA Resource field (name is related to the COM-port it is connected to). Click "Initialize!" and make sure the fields "dual/single" and "# of pixels" return the parameters of your used SLM model.

2. If a mapping file for the setup exists, load a mapping file by selecting the filename and click "Load". The graph should be visible in the right graph tab.

3. If a SLM response file exists, load it by selecting the file and click "Load". This file should also be visible in the graph to the right.

4. If one of the calibration files has not yet been created, refer to the next section for these tools.

5. Choose an option in the lower tab. Loading a pattern and defining an output pattern is available.

6. To load a pattern, select the file and click "Load". The pattern is visible on the graph. Clicking "Load pattern to SLM!" uploads it to the device.

7. To shape a desired waveform, select an input file, which should have been recorded before the input of the pulse shaper. Then, select a file with the desired waveform, which ideally uses the same timebase as the input signal. The desired time signal should not be shorter than the input signal, because no additional bandwidth can be generated by the pulse shaper. Clicking on "Load time signals" displays both signals to the left of the two graphs and the calculated spectra on the right graph. Then, "Shape!" uploads both patterns to the SLM masks and the output can be measured.

8. To use the feedback program, load a desired waveform which should be based on the same wavelength vector than the spectrometer, which is used as a feedback parameter, uses. Select a population size in one generation (number of chromosomes), and the probabilites for crossover and mutation. In the upper right corner, enter an integration time for the spectrometer. If the measurement shows saturation, reduce this value. Also, enter a left and right cut-off wavelength for the measurement to have a better range for visualization of the results. Click on "Optimize!", and the algorithm starts. The actual measured solution is visible on the graph on the right. Left to the graph is the status of the algorithm, that is the number of the present generation, the solution that is being examined and a graph of the last fitness factors. Also, a start solution can be used. Push the slide button to "Use" and enter the filename of the pattern which serves as a start solution. This can be stored in the Spectral shaping program.

A.5 Manual for the mapping program

1. Measure the output spectrum of the assembled beam with a spectrometer.

2. Choose a calibration vector and a smoothing function. For a polynomial function, choose its order too.

3. Click "calibrate". The program will turn individual pixels to its dark state and prompt for the corresponding transmission value. Enter the value from the spectrometer program with the large amplitude dip.

4. After finishing the calibration, the values are shown on the graph. Save the file for a later use in the control program.

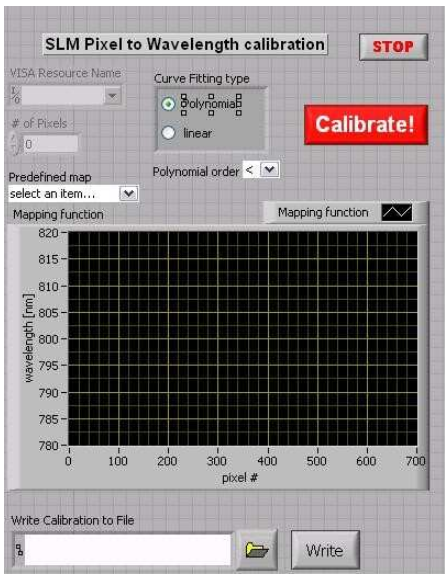

Figure A.2: Screenshot of the pixel to wavelength mapping calibration program.

A.6 Manual for the SLM response calibration program

1. Choose the number of datapoints that you would like to use for calibration. 128 are suitable for a quick overview, and 1024 datapoints take about 1.5 hours to complete, but the accuracy should be high enough for most purposes.

2. Select the VISA port which the oscilloscope is connected to and click "Calibrate". The program sends constant values to the whole frame and measures the transmission values. After calibration, the phase retardance of the liquid crystals is calculated.

3. Save the phase retardance to a file, which is required by the control program. The transmission values can be saved as well, but this is usually not necessary.

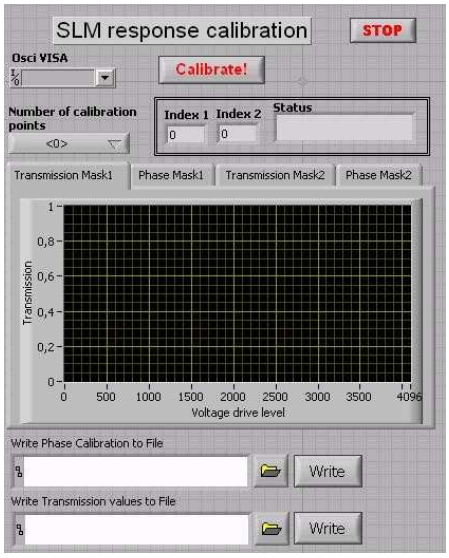

Figure A.3: Screenshot of the SLM response calibration tool.

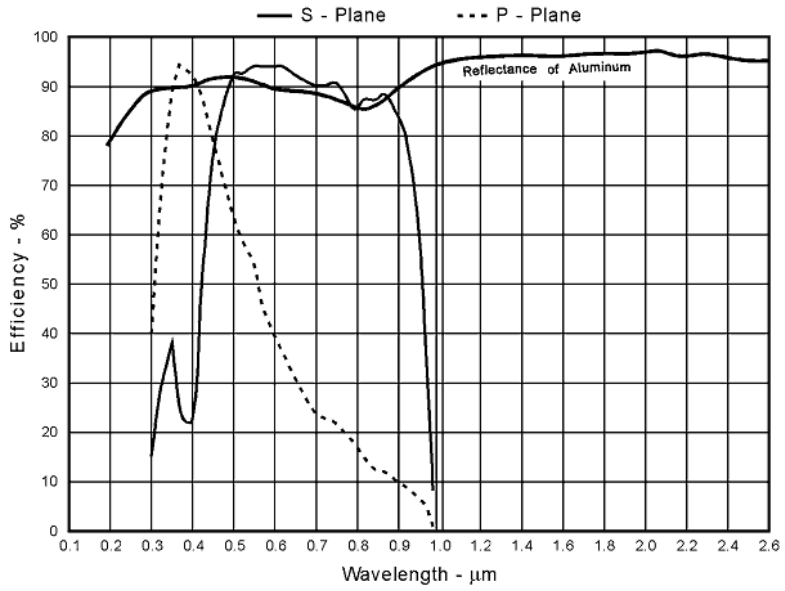

Figure A.4: Efficiency curve for the $2000\frac{1}{mm}$ Newport holographic grating

Bibliography

[BBS97] T. Baumert et. al.: *Femtosecond pulse shaping by an evolutionary algorithm with feedback*. Appl. Phys. B65, 779-782, 1997.

[BSG99] T. Brixner et. al.: *Feedback-controlled optimization of amplified femtosecond laser pulses*. Appl. Phys. B68, 281-284, 1999.

[Cam04] Cambridge Research & Instrumentation, Inc.: *Spatial Light Modulator (SLM) System*, CRi User's Manual, 2004

[ChC07] Chris Conery: *Introduction to Liquid Crystals*. Liquid Crystal Group University of Boulder, Colorado, USA. http://bly.colorado.edu/lcphysics/lcintro/tnlc.html.

[Fet99] M. R. Fetterman: *Ultrafast Pulse Shaping: Amplification, Characterization, and Applications*. Dissertation, Princeton University, 1999.

[Hof06] M. Hoffmann: *Novel Techniques in THz-Time-Domain-Spectroscopy*. Dissertation, University of Freiburg, Germany, 2006.

[KlF86] M. V. Klein, T. E. Furtak: *Optics*. Wiley, 1986.

[LeW01] Daniel E. Leiard, Andrew M. Weiner: *Femtosecond Direct Space-to-Time Pulse Shaping*. IEEE Journal of Quantum Electronics, Vol. 37, No.4, 2001.

[Lup04] Cosmin Lupulesco: *Femtosecond Analysis and Feedback Control of Molecular Processes in Organometallic and Alkaline Systems*. Dissertation, Freie Universität Berlin, 2004.

[Mic96] Zbigniew Michalewicz: *Genetic Algorithms + Data Structures = Evolution programs*. Springer, 1996.

[SaT91] B.E.A. Saleh, M.C. Teich: *Fundamentals of Photonics*. Wiley-Interscience, New York, 1991.

[SHF01] G. Stobrawa et.al.: *A new high-resolution femtosecond pulse shaper*. Applied Physics B 72, 627-630, 2001.

[ShG02] A. Sharan, D. Goswami: *Prospects of ultrafast pulse shaping*. Current Science, Vol. 82, No. 1, 2002.

[Tho07] Thorlabs, Diffraction grating specification, http://www.thorlabs.com/Thorcat/11700/11779-S01.pdf.

[Thu86] R. N. Thurston et. al.: *Analysis of Picosecond Pulse Shape Synthesis by Spectral Masking in a Grating Pulse Compressor*. IEEE Journal of Quantum Electronics, Vol. QE-22(5), 1986.

[Tre97] R. Trebino: *Measuring ultrashort laser pulses in the time-frequency domain using frequency-resolved optical gating*. Review of Scientific Instruments, 68(9), 1997.

[Tys00] Robert K. Tyson: *Adaptive Optics Engineering Handbook*. New York Marcel Dekker, Inc., 2000.

[PaL05] C. Palmer, E. Loewen: *Diffraction Grating Handbook*. Sixth edition, Newport Corporation, 2005.

[PWA03] A. Praekelt et. al.: *Compact, robust, and flexible setup for femtosecond pulse shaping*. Review of Scientific Instruments, 74(11), 2003.

[RWL92] D.H. Reitze, A.M. Weiner, D.E. Leaird: *Shaping of wide bandwidth 20 femtosecond optical pulses*. Applied Physics Letters **61** (11), 1992.

[Wei00] A. M. Weiner: *Femtosecond pulse shaping using spatial light modulators*. Review Article, Review of Scientific Instruments, Volume 71, Number 5, 2000.

[WeN95] M. M. Wefers, K. A. Nelson: *Analysis of programmable ultrashort waveform generation using liquid-crystal spatial light modulators*. Journal Optical Society America B, Vol. 12, No. 7, 1995.

[WLP92] A. M. Weiner et.al.: *Programmable Shaping of Femtosecond Optical Pulses by use of 128-Element Liquid Crystal Phase Modulator*. IEEE Journal of Quantum Electronics, Volume 28, Number 4, 1992.